

Targeted mutation of the gene encoding prion protein in zebrafish reveals a conserved role in neuron excitability

Valerie C. Fleisch^{a,b,1}, Patricia L.A. Leighton^{a,b,1}, Hao Wang^{a,b}, Laura M. Pillay^b, R. Gary Ritzel^b, Ganive Bhinder^b, Birbickram Roy^b, Keith B. Tierney^b, Declan W. Ali^b, Andrew J. Waskiewicz^b, W. Ted Allison^{a,b,*}

^a Centre for Prions and Protein Folding Diseases, University of Alberta, Edmonton, Alberta, T6G 2E9, Canada

^b Department of Biological Sciences, University of Alberta, Edmonton, Alberta, T6G 2E9, Canada

ARTICLE INFO

Article history:

Received 12 September 2012

Revised 8 February 2013

Accepted 13 March 2013

Available online 21 March 2013

Keywords:

NMDA receptor

Prion protein

Seizure susceptibility

Targeted mutagenesis

ABSTRACT

The function of the cellular prion protein (PrP^C) in healthy brains remains poorly understood, in part because *Prnp* knockout mice are viable. On the other hand, transient knockdown of *Prnp* homologs in zebrafish (including two paralogs, *prp1* and *prp2*) has suggested that PrP^C is required for CNS development, cell adhesion, and neuroprotection. It has been argued that zebrafish Prp2 is most similar to mammalian PrP^C, yet it has remained intransigent to the most thorough confirmations of reagent specificity during knockdown. Thus we investigated the role of *prp2* using targeted gene disruption via zinc finger nucleases. *Prp2*^{-/-} zebrafish were viable and did not display overt developmental phenotypes. Back-crossing female *prp2*^{-/-} fish ruled out a role for maternal mRNA contributions. *Prp2*^{-/-} larvae were found to have increased seizure-like behavior following exposure to the convulsant pentylenetetrazol (PTZ), as compared to wild type fish. In situ recordings from intact hindbrains demonstrated that *prp2* regulates closing of *N*-Methyl-D-aspartate (NMDA) receptors, concomitant with neuroprotection during glutamate excitotoxicity. Overall, the knockout of Prp2 function in zebrafish independently confirmed hypothesized roles for PrP, identifying deeply conserved functions in post-developmental regulation of neuron excitability that are consequential to the etiology of prion and Alzheimer diseases.

© 2013 Published by Elsevier Inc.

Introduction

Loss-of-function approaches that target disease-related genes have taught us much about the function of the cognate proteins in healthy brains, often leading to basic insights that inspire new therapeutic strategies. Despite much work on disease processes, the function of the prion protein in healthy brains has remained largely enigmatic. This is due in part to the lack of an overt developmental phenotype when *Prnp* is knocked out in mice (Bueler et al., 1992; Manson et al., 1994). On the other hand, several reports detail a phenotype when PrP homologs are transiently disrupted in zebrafish (Kaiser et al., 2012; Malaga-Trillo et al., 2009; Nourizadeh-Lillabadi et al., 2010), providing opportunity for insights into PrP's normal biological function.

Knockout of *Prnp* in mice produces viable animals with normal development (Bueler et al., 1992). This result suggested that gene redundancy with other prion-family genes such as *Shadoo* (*Sprn*) might exist,

but recent results showing normal development in *Prnp*^{-/-}; *Sprn*^{-/-} mice refute this (Daude et al., 2012). Phenotypes have been revealed during detailed analysis of adult *Prnp* knockout mice (Khalife et al., 2011; Steele et al., 2007). These include susceptibility to neuron death during insult with toxins or hypoxia, leading to the suggestion that PrP^C has a role as a neuroprotectant factor. Additionally, loss of PrP^C in mice leads to a susceptibility to seizures (Carulla et al., 2011; Rangel et al., 2007, 2009; Walz et al., 1999). The mechanisms whereby PrP^C can affect neuroprotection and seizures remain largely undefined, but could relate to a role for PrP in metal homeostasis, especially with respect to *N*-Methyl-D-aspartate (NMDA) channels (Khosravani et al., 2008a; You et al., 2012). Loss of homeostatic control of divalent metals at NMDA channels could accord with both excitotoxicity and increased neuron excitability/seizures (Stys et al., 2012).

In part because mouse *Prnp* knockouts have been intransigent towards relinquishing functions of PrP, other model systems have been interrogated. Transient knockdown of *Prnp* homologs in zebrafish has led to intriguing results from several research groups. Zebrafish possess two paralogs of the prion protein gene, *prp1* and *prp2*. Both predict protein products that are substantially larger than mammalian PrP^C, and thus comparisons on a sequence or amino acid level are difficult to interpret. However the zebrafish homologs share all the identified protein domains and post-translational modifications of mammalian

* Corresponding author at: Centre for Prions and Protein Folding Diseases, University of Alberta, Edmonton, Alberta, T6G 2E9, Canada. Fax: +1 780 492 9234.

E-mail address: ted.allison@ualberta.ca (W.T. Allison).

Available online on ScienceDirect (www.sciencedirect.com).

¹ Equal first authors.

PrP (Figs. 1C, S1), are glycosylated and are attached to the membrane with a GPI anchor when expressed in mammalian cell culture (Miesbauer et al., 2006). Further, at least *prp1* can be replaced by mammalian homologs to recover normal development (Kaiser et al., 2012; Malaga-Trillo et al., 2009), arguing for a substantial conservation of function.

To date, knockdown of *prp1* or *prp2* has been accomplished with morpholino oligonucleotide (MO) technology, which uses modified 25mer oligonucleotides expected to transiently block mRNA translation of the target gene. These reagents have been injected into embryos immediately after fertilization and are generally believed to be partially efficacious for approximately 3–4 days of development. This is sufficient time for zebrafish, which hatch after two days, to develop a functioning nervous system, but it remained unclear if more complete or longer-term disruption of prion gene(s) in zebrafish might reveal additional phenotypes. These works repeatedly demonstrated that substantial developmental deficits are induced by transient knockdown of *prp1* (Kaiser et al., 2012; Malaga-Trillo et al., 2009) or *prp2* (Malaga-Trillo et al., 2009; Nourizadeh-Lillabadi et al., 2010), including decreased cell adhesion, apoptotic cell death, arrested gastrulation, and impaired CNS development. Our recent work deployed zebrafish genetics and biochemistry of human homologs to link *prp1* with amyloid- β precursor protein (APP) in a niche role leading to CNS cell death (Kaiser et al., 2012). Thus data from zebrafish were consistent with an emerging function for PrP^C in excitotoxic cell death during Alzheimer disease progression as had been suggested by others (Lauren et al., 2009) and implicated a conserved role at synapses (Kaiser et al., 2012).

Intrigued by this collection of results, we sought to gain further insights into prion biology using an independent approach to disrupt the function of prion genes in zebrafish. Zebrafish *prp2* was prioritized for analysis because it is akin to mammalian homologs regarding abundant expression in the post-embryonic CNS (results herein and see Cotto et al., 2005; Malaga-Trillo et al., 2009), whereas the expression of its paralog *prp1* is primarily limited to early development (Cotto et al., 2005; Malaga-Trillo et al., 2009). Furthermore, it was noted that morpholino knockdown reagents against *prp2* failed to meet the most stringent tests of reagent specificity (e.g. rescue of phenotypes with cognate mRNA; see results herein, Malaga-Trillo et al., 2009), whereas MO reagents against *prp1* appear to be robust in this regard (Kaiser et al., 2012; Malaga-Trillo et al., 2009). Phenotypes were documented following targeted disruption of *prp2* via engineering of a custom zinc finger nuclease (ZFN). ZFNs are an emergent technology that, by analogy, represent a custom restriction enzyme designed to cut the target gene in vivo with good specificity; repair of the cut is error-prone and resultant insertions or deletions are heritable, producing an improper translation of the target protein. The mutant fish generated herein demonstrate that *prp2* disruption in zebrafish does not induce overt developmental phenotypes and revealed viable adult fish; this contrasts reports using *prp2* knockdown by morpholinos (Malaga-Trillo et al., 2009; Nourizadeh-Lillabadi et al., 2010) but is consistent with results reported in mice (Bueler et al., 1992) and other mammals (Richt et al., 2007; Yu et al., 2009). The targeted mutagenesis approach, though laborious, enabled characterization of phenotypes in post-embryonic zebrafish, including larvae with increased susceptibility to seizure-inducing drugs and coordinately disrupted NMDA receptor kinetics.

Materials and methods

Zebrafish husbandry and strains

Zebrafish of the AB strain were used as the wild type strain in this study, and this background was used for generation of *prp2* mutants. In some instances, *Tg(gfap:GFP)mi2001;mitfa^{w2/w2};roy^{as9/as9}* fish were used to examine CNS morphology in transparent ‘Casper’ fish

(combining mutant and transgenic lines ZDB-GENO-060623-2 (Bernardos and Raymond, 2006), with ZDB-ALT-990423-22 and ZDB-ALT-980203-444 (White et al., 2008)). Adult fish were maintained at 28 °C under a 14/10 h light/dark cycle and bred as described previously (Westerfield, 2000). Larvae were raised in E3 medium [containing 5 mM NaCl, 0.17 mM KCl, 0.33 mM CaCl₂, and 0.33 mM MgSO₄]. All protocols were approved the University of Alberta's Animal Care and Use Committee: Biosciences under the auspices of the Canadian Council on Animal Care.

ZFN target site selection and cloning of constructs

The zinc finger nuclease (ZFN) targeting methodology described previously (Meng et al., 2008) was adapted to create heritable mutations in zebrafish *prp2* (ZFin ID number ZDB-GENE-041221-3). The zebrafish *prp2* target site (5' cCACCTCCCTaccctgTGCTGGAGg 3', with ZFNs binding to the letters in capitals) was selected from a list of potential sites provided by the online algorithm which can be found on the website <http://pgfe.umassmed.edu/ZFPsearch.html>, based on the number of guanines, library diversities and other criteria described in the Results. Cloning of single finger oligos and target sites is described in the Supplemental Methods. An overview of the zinc finger nuclease selection is presented in Fig. S2 and described in the Results.

Bacterial one-hybrid selection of ZFNs

Library constructs and their corresponding target site constructs were co-transformed into the bacterial strain USO hisB- pyrF- rpoZ- (Addgene Plasmid 18049) using electroporation. Transformed cells were adapted to NM medium lacking histidine through several washes (Meng et al., 2008). Serial dilutions were spotted onto LB^{kana/carb} plates to determine transformation efficiency and the rest split up onto NM^{kana/carb} plates lacking histidine, one containing a low concentration and the other one containing a high concentration of 3-AT (typically in a range between 0.5 and 30 mM) to assay selection. Growth of colonies was assessed after 2–4 days, and if selection occurred (as indicated by observing fewer colonies on more stringent plates), 10–20 colonies were sequenced using the univF1 forward primer (see Supplemental Methods) to assess if selection had occurred.

ZFN combined library assembly and final selections

For each individual finger selection, approximately 100 colonies were picked, cultured for 2–3 h at 37 °C and DNA was prepared using a maxiprep kit (Qiagen # 12163). Library pools were amplified by PCR using phusion DNA polymerase (Thermo Scientific) and the univFx_forward/reverse primers (see Supplemental Methods). The following PCR program was utilized: 1 min initial denaturation at 98 °C followed by 40 cycles of 98 °C for 20 s, 58 °C for 15 s, 72 °C for 15 s plus a final extension at 72 °C for 10 min. Amplification products were run on a 1.5% agarose (TAE) gel, and bands of the appropriate size were excised and purified using a gel extraction kit (Qiagen 28706). In a second step, single finger pools were assembled with overlapping PCR using phusion DNA polymerase (Thermo Scientific) and the univF1_forward plus univF3_reverse primers (see Supplemental Methods and (Meng et al., 2008)). PCR products were again purified from an agarose gel and cloned into the 1352wUV2-kpn1-bamH1-stop vector (Addgene Plasmid 20704) using *Bam*HI and *Kpn*I. Assembled library diversities were expected to be about 10⁶ (as a result of randomly combining 100 colonies from each of F1, F2 and F3).

Combined library selections were performed as described above, however slightly higher 3-AT concentrations were used. Between 15 and 30 colonies were picked, their DNA extracted and sequenced to determine the optimal ZFN sequence binding to the specific DNA sub-site.

PrP2 transcript localization by *in situ* hybridization

Antisense riboprobe against the *prp2* transcript was generated by amplifying the template using primers that included a transcriptase binding site (5'-CGATGTAAATACGACTCACTATAGGGTGAGAATGTCA GTGTAGAAGGGA-3' and 5'-ATGGGTCGCTTAAACAATACTATTG-3'). This 1688 bp PCR product was used to template the production of DIG-labeled antisense riboprobe. Template for sense riboprobe control amplified the same region (primers 5'-TGAGAATGTCAGTGTAGAAGG GA-3' and 5'-CGATGTAAATACGACTCACTATAGGGATGGGTCGCTTAAACA TACTATTG-3'). Embryos or larvae were fixed in 4% paraformaldehyde with 5% sucrose in 0.1 M phosphate buffer pH 7.4 and stored at -20°C in MeOH. Hybridization methods were as previously described (Allison et al., 2010), except that excess riboprobe was incubated on the tissue for 48 h at 65°C , and signal development utilized 1:5000 anti-DIG-AP (Roche # 11093274910) and NBT and BCIP (4-Nitro blue tetrazolium chloride and 5-Bromo-4-chloro-3-indolyl phosphate, Roche # 11383213001 and 11383221001).

Immunohistochemistry and staining

Zebrafish at the various ages indicated were fixed in 4% paraformaldehyde with 5% sucrose in 0.1 M phosphate buffer pH 7.4. Immunohistochemistry was performed using standard protocols on intact larval fish or on material cryosectioned at $10\ \mu\text{m}$ as reported previously (Fraser et al., 2013). Fixed fish were washed sequentially with water, -20°C acetone, water and phosphate buffered saline pH 7.4 (PBS). Blocking was in 10% normal goat serum diluted in PBS with 0.1% TritonX-100. Primary antibodies applied were SV2 (previously established to label the synaptic vesicles and motor neurons in zebrafish, (Yazulla and Studholme, 2001), Developmental Studies Hybridoma Bank, ZDB-ATB-081201-1) and 3A10 (previously established to label a neurofilament, Mauthner neurons, and other subsets of neurons in the larval zebrafish (Hatta et al., 1991), Developmental Studies Hybridoma Bank, ZDB-ATB-090108-4). Primary antibodies were diluted 1:100 in PBS with 0.1% TritonX-100 and 2% normal goat serum. Secondary antibody was anti-mouse conjugated to AlexaFluor 555 (1:1000 Invitrogen #A31570) diluted in PBS with 1% TritonX-100, 1% Tween 20, 1% DMSO, and 2% normal goat serum. To-Pro-3 (Invitrogen T3605) diluted 1:5000 in the latter was used to stain nuclei. Phalloidin conjugated to AlexaFluor 546 (Invitrogen A22283), diluted in 1:100 in PBS with 0.1% Tween was used to stain actin. Images were acquired via confocal microscopy with Zeiss LSM 700 on Axio Observer.Z1, or on a Leica MZ16F stereomicroscope EL6000 mercury metal halide fluorescent light source and 12.8 megapixel digital camera (DP72, Olympus). Images were cropped/positioned in Powerpoint 2008 for Mac (Microsoft) and merged or manipulated for brightness and contrast in Zen confocal software (Zeiss), Photoshop CS3 and/or Imaris $\times 64\ 7.4.0$ (Bitplane).

Knockdown of *prp2* by delivery of morpholino oligonucleotide

Transient knockdown of *prp2* was performed by injection of morpholino oligonucleotide (MO) as previously described (Kaiser et al., 2012) using an MO directed against the 5' untranslated region of the *prp2* gene (5'-CTT CGG GCT GTT TTA AGC GAG TCC T-3', annotated at ZFin as ZDB-MRPHLNO-100423-7 from Malaga-Trillo et al., 2009). The binding site of this MO is contiguous with the ATG codon, and is thus very similar to the knockdown reagents in another study (shifted by 2 bp compared to "prp2-MO1", i.e. ZDB-MRPHLNO-101115-1) (Malaga-Trillo et al., 2009; Nourizadeh-Lillabadi et al., 2010). This MO was delivered to 1- or 2-cell stage zebrafish embryos at 4 ng dose, with or without 3 ng of *p53* morpholino (5'-GCG CCA TTG CTT TGC AAG AAT TG-3', ZDB-MRPHLNO-070126-7 (Langheinrich et al., 2002)) as indicated. In some instances, 225 pg of *prp2* mRNA was included in the injection solution, synthesized from a cDNA (accession # JQ994490) as described

previously (Kaiser et al., 2012). A standard control MO (5'-CCT CTT ACC TCA GTT ACA ATT TAT A-3') was delivered in some instances.

Determining relative transcript abundance using RT-qPCR

Experiments were performed in accordance with the MIQE guidelines (Minimum Information for Publication of Quantitative Real-Time PCR Experiments) (Bustin et al., 2009).

RNA isolation was performed on samples consisting either of pools of embryos/larvae ($n \approx 15\text{--}30$ individuals per pool, each pool typically collected from independent clutches of fish) at the age indicated or of individual brains from adult zebrafish. Samples were stored in RNAlater (Ambion AM7021) at 4°C until RNA extraction. Total RNA was extracted from pools of embryos using the RNeasy Kit (Qiagen 74104) and manufacturer's protocols using 600 μL of Buffer RLT containing 1% β -Mercaptoethanol and homogenizing with a rotor stator homogenizer (VWR 47747-370), and on-column DNase digestion was performed using Qiagen DNase I. Total RNA was extracted from adult brain by homogenizing in 1 mL of QIAzol lysis reagent (VWR 47747-370), on-column DNase digestion and using an RNA easy Lipid Tissue Mini Kit (Qiagen 74804). Absence of genomic DNA contamination in each RNA preparation was assessed by examining melt curves and by using primers against *APPb* exons 3 and 4 (5'-GCCAACCAGCCTGTCCAGCAT-3' and 5'-GCCAGTGTAGAT GACTCTCG-3'); If genomic DNA had been present, a 477 bp band would have been detected in addition to the constitutive 205 bp mRNA band. RNA quantity was determined using a Nanodrop spectrophotometer (GE Healthcare 28 9244-02). All of the samples had similar rRNA profiles and RNA integrity numbers (RIN values of 8.4 or greater when reported) as determined using an Agilent RNA 6000 NanoChip and Agilent 2100 Bioanalyzer.

cDNA was generated using a Long Range 2 Step RT-PCR Kit (Qiagen 205922) using oligo dT primers and Long Range Reverse Transcriptase. The reaction volume was 20 μL , with either 1 μg total RNA or a no template control.

Quantitative PCR was performed using a 7500 Real-Time PCR system (ABI Applied Biosystems). Transcript abundance for *prp2* as well as *prp1*, *appa*, *appb*, *tp53*, and *ccng1*, was assessed relative to β -actin and *ef1 α* . The latter two reference genes were chosen based on past literature optimizing RT-qPCR in zebrafish (Casadei et al., 2011; Tang et al., 2007). RT-qPCR primers were designed using Primer Express 3.0 and verified with a standard curve. Primers were designed in the 3' exons of each gene, and are expected to amplify all splice variants in all genes except *p53* (Table S4). Primer sequences and efficiencies are available in Supplementary Tables S4 and S5, respectively. Melting dissociation curves were performed to assess primer specificity, and the presence of a single peak indicated that there was a single product for each primer set and no primer dimers. RT samples were subsequently analyzed at a 24-fold dilution with C_t values ranging from 15 to 30. qPCR reactions were performed with 3 technical replicates of each biological replicate (3–4 biological replicates, each consisting of either separate pools of embryos or tissues dissected from an individual adult fish). Individuals completing these experiments were blinded to the genotype and MO-treatment of the samples prior to beginning the RNA isolation protocol.

Each reaction contained 5 μL Dynamite Master Mix (Molecular Biology Service Unit, University of Alberta, including SYBR Green and platinum Taq hot start enzyme (Invitrogen)), 2.5 μL of pre-mixed primer set, and 2.5 μL cDNA for a total volume of 10 μL . After an initial denaturation step (2 min at 95°C), cycling consisted of 40 cycles of 95°C for 15 s followed by 60°C for 1 min. One cycle for melting dissociation curve analysis followed these 40 cycles and consisted of 95°C for 15 s, 60°C for 1 min, 95°C for 15 s, and finally 60°C for 1 min. Data analysis was performed using 7500 Software for 7500 and 7500 Fast Real Time PCR Systems version 2.0.1 (AB Applied Biosystems) with auto C_t calling. Transcript abundance was normalized to *ef1 α* and reported with β -actin

levels normalized to 1. Relative fold change in transcript abundance was analyzed by *t*-test performed with SYSTAT 12 (Chicago, IL) on the resulting RQ values.

Behavioral analysis of PTZ-induced seizures

Established assays (Baraban et al., 2005, 2007; Bustin et al., 2009) measuring stage I and II seizures were performed. Behavioral tracking software quantified the movement of zebrafish larvae arrayed in a 96-well plate. For trials involving 5 days post fertilization (dpf) *prp2*^{-/-} mutants and siblings, larval fish were first acclimatized in E3 medium for 20 min and then subjected to 2.5 mM PTZ (pentylene-tetrazol, Sigma-Aldrich #P6500) for 20 min to analyze the response to the convulsant (Baraban et al., 2005, 2007; Bustin et al., 2009). Some trials were performed on embryos from breeding of *prp2*^{+/-} fish followed by genotyping the *prp2* locus, whereas other trials involved breeding *prp2*^{-/-} fish and comparing them to AB fish (the background used to generate the ua5001 allele). For trials involving 3 dpf larvae, fish were acclimatized in their typical growth media (E3 medium) for 30 min and subsequently subjected to 2.5 mM PTZ for 30 min. Swimming behavior during both acclimation and PTZ exposure was monitored. Fish were monitored individually in single wells of a 96 well, flat bottom plate in 100 or 200 μ L of fluid. The plate was placed on a light box with an overhead video recording and tracking system. Motion was captured at 30 frames per second using a high resolution camera (SX-920C-HR; Matco Canada, St. Laurent, QC) connected to a video capture card (Picolo H.264; Euresys, San Juan Capistrano, CA) in a PC running EthoVision® XT7 software (Noldus, Wageningen, Netherlands), as described previously (Bhinder and Tierney, 2012). Researchers were blinded to fish genotype throughout the behavioral assessment. After tracking the fish movement, raw data (30 data points/second/fish) were exported to Microsoft Excel to calculate swimming speed and distances traveled transformed into 10 s time bins. The average velocity, excluding data points generated when the fish were out of view from the camera, was calculated during two time periods consisting of the final 15 min of the acclimation period, and minutes 5–20 following PTZ addition. Movement following addition of convulsant (2.5 mM PTZ) was normalized to the movement of the larva during an acclimation period prior to addition of convulsant. These values were tested for significance using Kruskal Wallis or Mann–Whitney U tests in Systat 12.

In situ analysis of NMDA receptor kinetics

Recordings from 2 dpf larvae utilized a preparation with intact trunk, spinal cord and hindbrain as previously described (Patten and Ali, 2009; Patten et al., 2010). Larvae were anesthetized in MS-222 (Sigma-Aldrich) prior to dissection and subsequently paralyzed in 15 μ M D-tubocurarine (Sigma-Aldrich) in an aerated perfusion bath held at 20–24 °C lacking MS-222. Maternal zygotic *prp2*^{-/-} larvae, lacking maternal contribution of *prp2* mRNA, were compared to wild type larvae. Miniature excitatory post-synaptic currents (mEPSCs) were recorded from the Mauthner cell, which is readily identified using DIC microscopy. Recording conditions were as reported previously (Patten and Ali, 2009; Patten et al., 2010), including use of 1 μ M tetrodotoxin to block action potentials. The spontaneous whole cell currents, representing AMPA and NMDA excitatory post-synaptic currents, were recorded with a holding potential of +40 mV with 5 μ M strychnine and 100 μ M picrotoxin to block γ -aminobutyric acid and glycine receptors. NMDA receptor currents were confirmed with the use of the NMDA receptor antagonist 2-amino-5-phosphonovalerate (APV, 50 μ M) which abolished NMDA receptor activity. NMDA mEPSCs returned upon wash out of APV. Currents were amplified with an Axopatch 200B Amplifier, low-pass filtered at 5 kHz (–3 dB) and digitized at 50 kHz to accurately record both NMDA and AMPA mEPSCs (if necessary). Synaptic events were first examined visually, and were

then detected and analyzed using AxoGraph X (MDS Analytical Technologies, Sunnyvale CA). Decay kinetics were analyzed by fitting a sum of exponential curves over the first second of the decay phase. Rise time was calculated as the time between reaching 20% and 80% of the current amplitude. In a subset of animals from each genotype, small changes in the recording parameters during the session (drifting access resistance of the pipette) precluded confident analysis of event amplitude or kinetics, though these recordings were used to accurately assess NMDA event frequency. Quantifications were compared between genotypes using *t*-tests in SigmaStat (Systat Software, San Jose CA).

Results

Targeted disruption of *prp2* in zebrafish using zinc finger nucleases

ZFN technology (Meng et al., 2008) was adapted to create heritable mutations in the zebrafish *prp2* gene, ZFin ID number ZDB-GENE-041221-3. A suitable ZFN target site within the gene was identified with assistance of an online algorithm (Meng et al., 2008). The criteria for target site selection included high guanine content, amenable ZFN library diversities (below 10⁷) and, most importantly, the position of the target site in the gene relative to the functional protein domains. The *prp2* ZFN target site selected based upon these criteria, 5'-CACCTCCCTaccctgGTGCTGGAG-3', consisted of two regions of 9 base pairs each, separated by 6 base pairs (Fig. 1B). Thus the engineered ZFN enzyme has an 18 bp recognition site and is predicted to specifically bind to a single location within the genome. The selected site is located immediately 5' of the repeat region of the *prp2* gene (Figs. 1 and S1), and mutations in this sequence (e.g. small deletions caused by the error-prone non-homologous end joining repair process initiated by ZFN cutting) resulting in frame-shifts are predicted to produce a non-functional, truncated prion protein. No alternative start sites were detected in this gene by in silico analysis, and the selected target is present in all splice variants (indeed only one variant is known, with the coding region contained in a single exon).

To engineer a ZFN that would specifically bind this *prp2* target site, two stages of bacterial-one-hybrid selection were performed on libraries of potential zinc fingers (an overview is schematized in Fig. S2, and the resultant fingers were subsequently fused to a nuclease domain). Details of Methods are provided in the Supplementary materials. Zinc fingers that exhibited strong binding to their target site were identified as those that enabled growth of bacteria in the bacterial-one-hybrid selection system (Meng et al., 2008). A library encoding each of the candidate single zinc fingers (three libraries of 5p fingers and three libraries of 3p fingers) was generated by cloning oligonucleotides. These oligonucleotides encoded zinc finger proteins with randomization of amino acid identities at several sites known to effect DNA binding, as suggested by the algorithm (Fig. S2).

Zinc fingers that were good candidates for *prp2* target site binding, as identified by one or two stages of bacterial-one-hybrid selection, were then subjected to functional characterization (two candidate 5p, and five candidate 3p. Supplemental Methods, Table S2, S3). These arrays of zinc fingers were cloned into expression constructs containing the nuclease domain from *FokI*, and tested for cutting proficiency in concerted combinations. To preclude time-consuming in vivo testing, screening was performed to ascertain if they successfully cut their target DNA in vitro (Supplemental Methods). As expected, the PrP2 ZFNs cut their respective target sites in a specific fashion (an example is presented in Fig. S3).

To deliver the ZFNs to zebrafish embryos, ZFN mRNA was transcribed from one 5p ZFN and two different 3p ZFNs (Tables S2 and S3), and injected in combinations into single-cell stage zebrafish embryos. Only one of the two tested combinations induced genomic mutations (Tables S2 and S3). The observed frequency of insertion and deletion mutations, primarily small deletions of 1 to 8 base pairs, was

4.6% (6/130 tested clones; Fig. S3). A smaller number of single base pair substitutions were also observed.

To isolate zebrafish carrying *prp2* mutations, embryos injected with this ZFN pair were raised until adulthood, and germ line transmission of the mutation was examined by crossing adult zebrafish and genotyping their offspring. As before, genomic DNA of $n = 10$ larvae at 24 hpf was isolated from each clutch, and an amplicon containing the target site was sub-cloned to assess the occurrence of mutations. One pair of adult zebrafish was found to give rise to embryos carrying a 4 base pair deletion, which was designated as the allele *ua5001* (Fig. 1E). Offspring from this pair were raised (producing the F1 generation) until adulthood and tested for heterozygosity by fin-clipping and sequencing. In-breeding of identified heterozygous F1 carriers ($n = 4$ fish) revealed larvae exhibiting a Mendelian inheritance pattern of the mutation. Larvae from three clutches were sequenced to determine their genotypes ($n = 55$ larvae: 15 *prp2*^{+/+}, 27 *prp2*^{ua5001/+}, and 13 *prp2*^{ua5001/ua5001}) and the allele inheritance patterns were not different than the expected Mendelian ratios (27%, 49% and 24%, respectively. χ^2 test = 0.164, $p = 0.92$).

Disruption of *prp2* by ZFN does not produce an overt developmental phenotype

The frameshift in translation caused by the 4 base pair deletion in the *prp2*^{ua5001} allele is predicted to result in a null allele, as all protein domains recognizable in the primary sequence of the mature protein are lost (compare Figs. 1D with 1C). Previous efforts aimed at understanding prion protein biology via *prp2* loss-of-function in zebrafish utilized morpholino knockdown. These annotated cell death and disrupted head morphology (Malaga-Trillo et al., 2009; Nourizadeh-Lillabadi et al., 2010), which are phenotypes we also observed with these MO reagents (see below). This was in sharp contrast to the fish observed following crosses of *prp2*^{ua5001/+} heterozygous fish; these larvae lacked any overt phenotypes throughout development (Fig. 1F). Sequencing confirmed that approximately 25% of these phenotypically normal fish were homozygous *prp2*^{ua5001/ua5001} (Fig. 1E).

Maternal contributions of *prp2* mRNA do not account for normal development

We were intrigued by the disparity in observed phenotypes when *prp2* was disrupted by MO knockdown as compared to ZFN-induced targeted mutation, and set out to examine alternative hypotheses: (i) Maternal contributions of *prp2* mRNA into the egg are sufficient for normal development in *prp2*^{ua5001/ua5001} fish; (ii) The various *prp2* MO knockdown reagents deployed are efficacious but also induce phenotypes that are not specific to *prp2* disruption; and (iii) The mutation in *prp2*^{ua5001/ua5001} fish fails to disrupt the normal gene product. In subsequent sections we examine the latter, and here we investigate the former. The *prp2* MO reagents that produce phenotypes are designed to block translation of both maternal and zygotic mRNA. Robust expression of *prp2* mRNA can be detected in recently fertilized zebrafish embryos (Fig. 2A). These observations accord with a role for maternal deposition of wild type *prp2* mRNA, and thus masking of phenotypes during breeding of *prp2*^{ua5001/+} fish was deemed possible.

It was noted that both male and female *prp2*^{ua5001/ua5001} fish were viable into adulthood and had survival rates not different from wild type fish (Figs. 2B, C). Breeding *prp2*^{ua5001/ua5001} fish did not suggest any deficits in fecundity. The oldest *prp2*^{ua5001/ua5001} fish we had raised at time of writing was 18 months old, and exhibited no apparent deficits, suggesting that at least some *prp2*^{ua5001/ua5001} fish can thrive in a manner indistinguishable from wild type fish (adulthood is considered the time of sexual maturity, ~3 months of age, and the normal lifespan of a zebrafish is 3–5 years). *prp2*^{ua5001/ua5001} males and females were crossed to generate *prp2*^{ua5001/ua5001} fish lacking the hypothesized

maternal contribution of wild type *prp2* mRNA. Zebrafish lacking both maternal and zygotic contributions of a gene are defined as ‘maternal zygotic’ mutants, as compared to zygotic mutants that do not lack maternal gene function. These maternal zygotic mutant progeny appeared normal (Fig. 2D), and thus maternal mRNA contributions can be excluded as having a causal role in the normal development of *prp2*^{ua5001/ua5001} fish, i.e. maternal *prp2* mRNA does not account for differences between the mutant and morphant phenotypes. Hereafter *prp2*^{ua5001/ua5001} genotypes are denoted as “*prp2*^{-/-}”. Subsequent back-crosses of homozygous mutant fish to date have supported this conclusion through to the F5 generation.

prp2 expression is disrupted in *prp2*^{-/-} fish

An alternate interpretation of the normal development observed in *prp2*^{ua5001/ua5001} fish is that the mutation does not disrupt the Prp2 protein. This is unlikely, as described above, because the mutation induces a frame-shift early in the *prp2* coding region, predicting a truncated molecule lacking all the recognizable protein domains that form the mature molecule (see Figs. 1 and S1). Multiple attempts to generate an antibody against Prp2 protein were not successful, and no cross-reactivity was observed when commercial antibodies against mammalian PrP^C were investigated. Instead the abundance of *prp2* transcripts was assessed in the mutants, because RNA surveillance can reduce transcript levels via nonsense-mediated decay (Culbertson, 1999). This mechanism is especially robust in transcripts harboring premature termination codons in the first coding exon. Nonsense-mediated decay is a conserved mechanism to remove abnormal transcripts encoding truncated proteins, and generally occurs when a premature termination codon is located more than 50–55 nucleotides upstream of an exon–exon boundary (Maquat, 2004). The mechanisms of nonsense-mediated decay are conserved and often observed in embryonic zebrafish mutants (reviewed in Wittkopp et al., 2009).

Transcript abundance was determined by RT-qPCR carried out as per MIQE guidelines (Bustin et al., 2009). Integrity of extracted RNA was good regardless of genotype (Figs. 3D, S4), and the RT-qPCR reagents we deployed detected a single product (examples of melt curves in Fig. 3E) in a linear range (Figs. 3F, S4). Other aspects ensuring integrity of the RT-qPCR methods are reported in the Methods and associated Supplementary Tables. Multiple biological replicates were compared regarding expression of several genes relative to the reference gene *ef1 α* . Biological replicates consisted of pools of ~20 larvae, or represented brains of individual adult fish.

The abundance of *prp2* mRNA is 6-fold reduced in *prp2*^{ua5001/ua5001} larvae compared to *prp2*^{+/+} larvae at 48 hpf (Fig. 3G, $p < 0.01$). An additional reference gene, β -actin, did not change in abundance relative to *ef1 α* levels, nor did any of the five other genes tested (see below). Similar results for *prp2* abundance, including 4- to 6-fold decreases, were observed in 5 day old larvae and adult brains (Fig. S5, $p < 0.001$).

prp2 expression was also assessed by in situ hybridization. The results confirmed past work showing that *prp2* transcripts are abundant in the zebrafish CNS (Malaga-Trillo et al., 2009) (Fig. 3). Consistent with the RT-qPCR results, *prp2* transcripts were markedly reduced in *prp2*^{ua5001/ua5001} larvae compared to *prp2*^{+/+} larvae (Figs. 3A–C). Thus, in addition to a predicted disruption of translation that severely truncates the protein, the *ua5001* allele leads to decrements in *prp2* transcript abundance consistent with nonsense-mediated decay and a null allele.

Expression of related genes is not perturbed in *prp2*^{-/-} fish

Alternate explanations for decreases in *prp2* transcript abundance in *prp2*^{-/-} fish could include an idiosyncrasy of the methods, or a general decrement in CNS/synapse transcript abundance might be expected from improper development or degeneration of tissues.

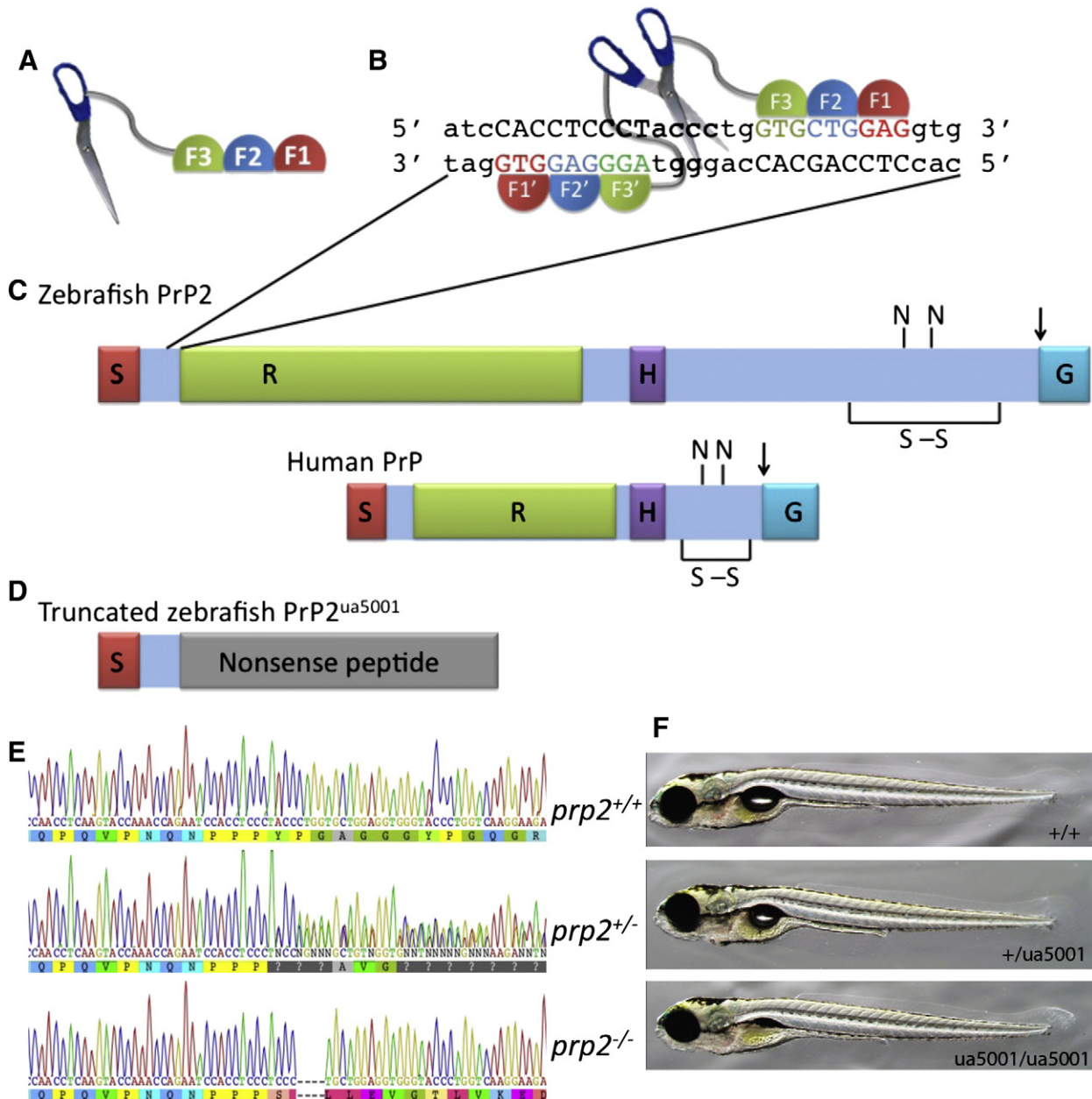


Fig. 1. Targeted mutation of *prp2* in zebrafish by a custom zinc finger nuclease (ZFN) reveals no overt developmental phenotype. **A.** The ZFNs deployed consisted of three zinc fingers (F1, F2, F3) fused to half of an endonuclease domain (represented by a single blade of a pair of scissors). **B.** Each ZFN was engineered via bacterial-one-hybrid selection to bind specifically to a 9-base pair recognition site in the DNA (in CAPS, see also Fig. S2) within the zebrafish *prp2* gene, creating an 18-base pair site predicted to occur only once in the genome. These two ZFN components heterodimerize to form an endonuclease and cut the *prp2* gene; repair of this cut is error-prone, leading to heritable changes including small deletions. **C.** Zebrafish Prp2 protein is larger than its mammalian homologs but they share all protein domains identifiable in the primary sequence (see also Fig. S1). The ZFN target site occurs before the amino-terminus of the first recognizable domain (R, Repeat domain) of the mature protein (S, Signal peptide; H, Hydrophobic domain; N, glycosylation site; S–S disulphide bond; G, GPI Signal Sequence; arrow, location of GPI anchor (see also Cotto et al., 2005)). **D.** The ua5001 allele generated by ZFN mutagenesis has a four base pair deletion at the target site, leading to a frameshift and predicts non-functional protein including elimination of the repeat domain followed by a nonsense peptide, i.e. a string of amino acids lacking any similarity to known proteins. **E.** Sequencing of genomic DNA at the ZFN target site within *prp2*, from larvae acquired by breeding *prp2*^{ua5001/+} fish, reveals a 4 base pair deletion in heterozygous and homozygous states. Predicted translation is presented below each trace, showing the difference between mutant and wild type, whereas this is not discernible in some of the middle trace due to the heterozygous state making nucleotide calls impractical. **F.** *prp2*^{ua5001/+} and *prp2*^{ua5001/ua5001} larvae lack any overt developmental phenotype (examples shown are 7 days post-fertilization).

We tested this by assessing genes with similar biological roles and/or distributions of expression compared to *prp2*. These included RT-qPCR analysis of *prp1*, *appa*, and *appb* (the latter are homologs of the Alzheimer disease gene amyloid- β precursor protein APP). None of these genes were altered when comparing their abundance between genotypes in three developmental stages (Figs. 3, S5). Thus, amongst the eight genes tested (including the reference genes and two others below), decreases in gene transcript

abundance were observed only for *prp2*, supporting the robust specificity of the assays. The results are consistent with the lack of any morphological or neurodegenerative phenotype observed in the CNS.

Previous work analyzing transcript levels in zebrafish injected with either of two *prp2* morpholinos reported an increase in abundance of *tp53* transcripts, encoding the cell-death-related protein p53 (Nourizadeh-Lillabadi et al., 2010). This is consistent with

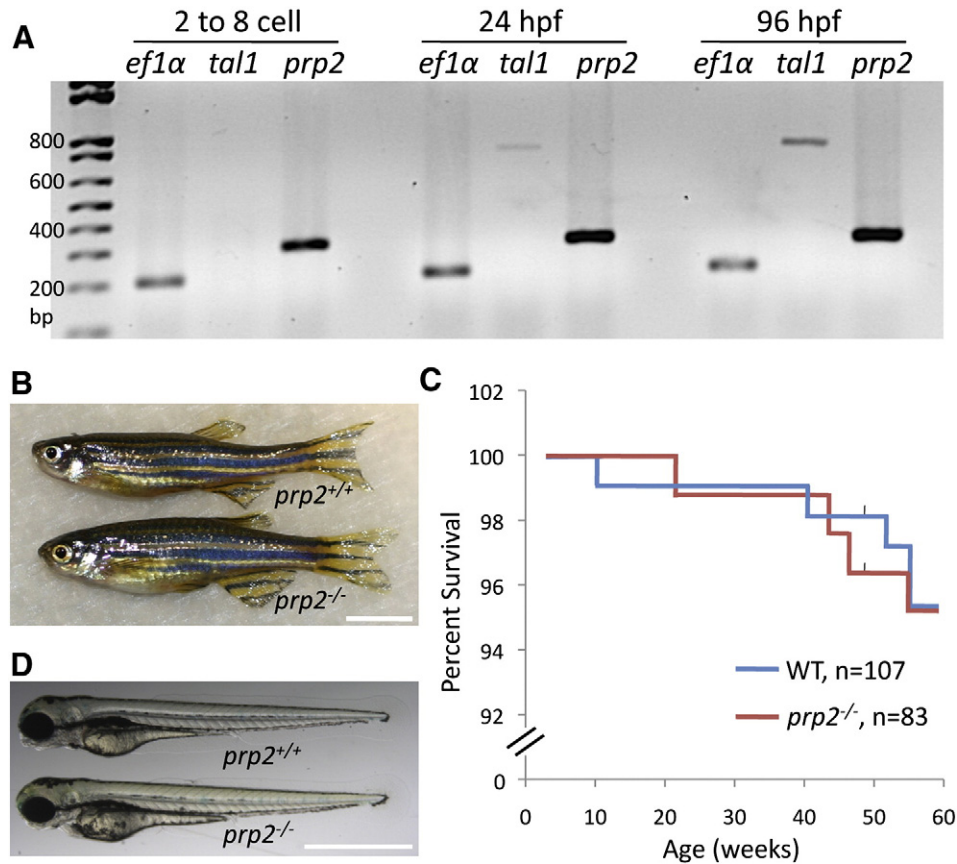


Fig. 2. Maternal contribution of *prp2* mRNA does not account for lack of overt phenotype. **A.** *prp2* transcripts are present in recently-fertilized wild type zebrafish embryos. Three developmental stages are presented: 2–8 cell stage, 24 h post-fertilization (hpf) and 4 days post-fertilization (dpf). Transcripts that are known to be present at high and low abundance in zebrafish eggs (*ef1α* and *tal1*, respectively) are presented for comparison. **B.** *Prp2*^{ua5001/ua5001} fish survive until adulthood and present no apparent phenotype. Scale bar = 0.5 mm. **C.** Kaplan–Meier survival curves of fish from breeding of *prp2*^{ua5001/ua5001} (= *prp2*^{-/-}) fish, vs. wild type (WT) strain-matched AB fish (Supplemental Methods). Data censure at 48 weeks is a consequence of two ages of fish being quantified; the experiment began with *n* = 22 and *n* = 17 fish from *prp2*^{ua5001/ua5001} and AB genotypes, respectively, and the remainder of the fish were added to the experiment 11 weeks later. **D.** Maternal zygotic mutants, derived from breeding female *prp2*^{ua5001/ua5001} fish, produces normal larvae; thus maternal contribution of *prp2* mRNA cannot account for the normal development of larvae. Maternal zygotic *prp2*^{ua5001/ua5001} larvae shown at 3 days post-fertilization (bottom), compared to wild type larvae (top). Scale bar = 1 mm.

cell death observed in the head region of *prp2* morphants (Malaga-Trillo et al., 2009; Nourizadeh-Lillabadi et al., 2010). This was replicated herein, in that the use of *prp2* MO demonstrated abundant cell death and a three-fold increase in *tp53* abundance (Fig. S6C). This contrasts *prp2*^{ua5001/ua5001} fish at 48 hpf that demonstrated no such change in *tp53* levels compared to wild type fish (Fig. 3G), consistent with the lack of overt cell death in developing mutant embryos. Parallel observations were noted in the *ccng1* transcript, encoding Cyclin G1 that itself regulates p53 (Jost et al., 1997), in that *ccng1* was more abundant in 48 hpf *prp2* morphants (Nourizadeh-Lillabadi et al., 2010) but was equally abundant in wild type and *prp2*^{ua5001/ua5001} 48 hpf larvae (Fig. 3G). Increased abundance of *tp53* transcript following delivery of a morpholino reagent to zebrafish is typically interpreted as a lack of reagent specificity, often representing the MO reagents causing developmental deficits via off-target effects (Robu et al., 2007). Indeed inclusion of a MO blocking *tp53* in the injection solution was able to rescue the cell death phenotypes observed in *prp2* morphants (Fig. S6). A lack of specificity in the available *prp2* MO reagents is also consistent with results from several groups that fail to rescue *prp2* MO-induced phenotypes using cognate *prp2* mRNA ((Malaga-Trillo et al., 2009; Nourizadeh-Lillabadi et al., 2010), see also Fig. S6F). Indeed *prp2* mRNA is able to partially rescue *prp1*, but not *prp2*, MO-induced phenotypes (Malaga-Trillo et al., 2009), and thus the *prp2* mRNA delivery is likely a robust test of *prp2* MO fidelity (or lack thereof). This contrasts results for the

zebrafish paralog *prp1*, wherein *prp1* morpholino induced phenotypes have been demonstrated to be specific to the knockdown reagent because either cognate mRNA or mammalian *Prnp* mRNAs are able to rescue developmental deficits (Kaiser et al., 2012; Malaga-Trillo et al., 2009). In sum, it appears that previously reported phenotypes resulting from *prp2* knockdown are due, in part, to off-target effects of the morpholino reagents; such observations are becoming widespread amongst morpholino papers (Bedell et al., 2011), thus necessitating caution when controls cannot prove reagent specificity (Eisen and Smith, 2008). The disparity of phenotypes between *prp2* morphant fish and *prp2*^{ua5001/ua5001} mutant fish is also consistent with this interpretation.

It is noteworthy that although the specificity of the *prp2* MO reagents is not supported herein, the efficacy of the reagent in partially reducing *prp2* abundance is supported by two lines of evidence. Past work shows *prp2* MO can reduce both protein and transcript abundance (Nourizadeh-Lillabadi et al., 2010) and data herein at least supports the latter (Fig. S6). Thus it appears that while *prp2* can be disrupted effectively by *prp2* MO reagents, the previously reported phenotypes are not caused by this disruption. This conclusion is supported by the normal development of *prp2* mutants, despite the reduction of *prp2* transcript in *prp2*^{ua5001/ua5001} mutants being greater in magnitude compared to that observed in the morphants (Fig. S6). Thus discrepancies between *prp2* morphants and mutants are most consistent with the interpretation that *prp2*^{ua5001/ua5001} mutants represent a null allele, and this is also consistent with a lack

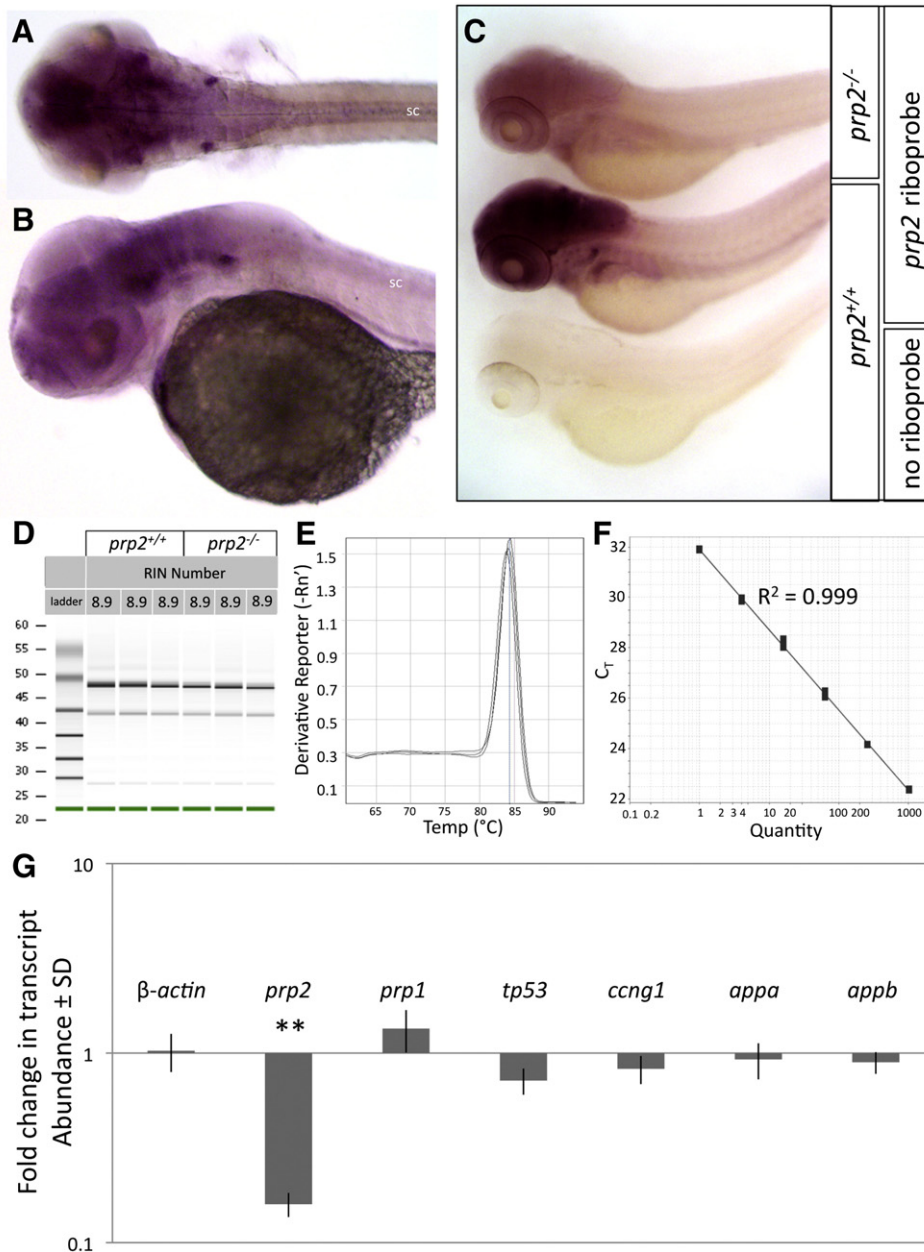


Fig. 3. *Prp2* transcript is less abundant in *prp2*^{ua5001/ua5001} zebrafish compared to wild type. A, B. In situ hybridization with riboprobe against *prp2* transcript in wild type zebrafish 2 days post-fertilization showing *prp2* transcript (purple) is abundant in the CNS. Anterior is to the left. Panel A is a dorsal view, with the yolk sac removed. Panel B is a lateral view. sc, spinal cord. C. *Prp2* transcript is less abundant in *prp2*^{-/-} larvae (top) compared to *prp2*^{+/+} larvae (middle). *prp2*^{+/+} larvae treated identically except for receiving no riboprobe is presented to assess background staining levels; control for labeling specificity using sense riboprobe also shows low background staining (Fig. S5). D–F. Examples of quality assessment regarding the RT-qPCR analysis, which was performed on all RT-qPCR reagents, including the quality of total RNA assessed by Bioanalyzer being similar regardless of genotype with RNA integrity numbers (RIN) reported above each lane (D), three melting dissociation curves for *prp2* transcript at 1/16th dilution to assess qPCR reaction integrity (E), and a plot of C_t values vs. concentration (3 technical replicates presented per dilution) for dilutions of the template demonstrates linearity and high correlation coefficient ($R^2 = 0.999$). See also Fig. S4. G. Quantification of transcript abundance demonstrates *prp2* is 6-fold decreased in *prp2*^{ua5001/ua5001} compared to *prp2*^{+/+} larvae at 2 dpf, whereas other genes analyzed had equal abundance regardless of genotype. Data normalized to reference gene *ef1a* and presented as fold change of mutant relative to wild type. Samples were independent biological replicates each of which consisted of pools of larvae from different parents, $n = 3$, ** $p = 0.002$.

of phenotypes when *Prnp* is knocked out of mice (Bueler et al., 1992) or other mammals (Richt et al., 2007; Yu et al., 2009).

Characterization of neuronal and glial markers fails to reveal phenotypes in *prp2*^{-/-} fish

With an aim of exploring for phenotypes amongst neurons and glia, we examined larvae generated from breeding of *prp2*^{-/-} fish using immunohistochemistry and/or transgene expression. To better

visualize the CNS in fish lacking pigment, we established wild type and *prp2*^{ua5001/ua5001} adults expressing GFP under control of the GFAP promoter (Bernardos and Raymond, 2006) on the 'Casper' background of fish that lack reflective iridophores and melanin pigment throughout their body (excepting the eyes) (White et al., 2008). Thus *Tg(gfap:GFP)mi2001;mitfa*^{w2/w2}; *roy*^{a9/a9}; *prp2*^{ua5001/ua5001} adults were crossed and progeny examined at various ages compared to the same background with wild type *prp2*, i.e. *Tg(gfap:GFP)mi2001;mitfa*^{w2/w2}; *roy*^{a9/a9}; *prp2*^{+/+}. This permitted inspection of organ morphometry in

a fluorescent stereomicroscope, especially including unprecedented detail being visible with live imaging in the post-larval CNS. No differences in brain morphometry were noted between genotypes (Figs. 4 and S7). Increase in GFAP abundance in the form of gliosis is an early and sensitive outcome of neurodegeneration (Middeldorp and Hol, 2011). No difference in the intensity of GFP expression, driven by the GFAP promoter, was apparent (examples at 7 and 21 dpf in Figs. 4 and S7). Staining of nuclei with To-Pro-3

visualized in whole embryos at 2 dpf or in sectioned material at 7 dpf using confocal microscopy revealed no apparent difference in abundance of pyknotic nuclei (Figs. 5B, E). Markers of synapses and neuron subpopulations that have previously been shown to be sensitive to disrupted neurodevelopment and neurodegeneration (Lemmens et al., 2007) were not different between *prp2* genotypes (Figs. 5K–N). We found that the synaptic marker SV2 labeled the same axons as GFAP:GFP fluorescence in the primary motor neurons,

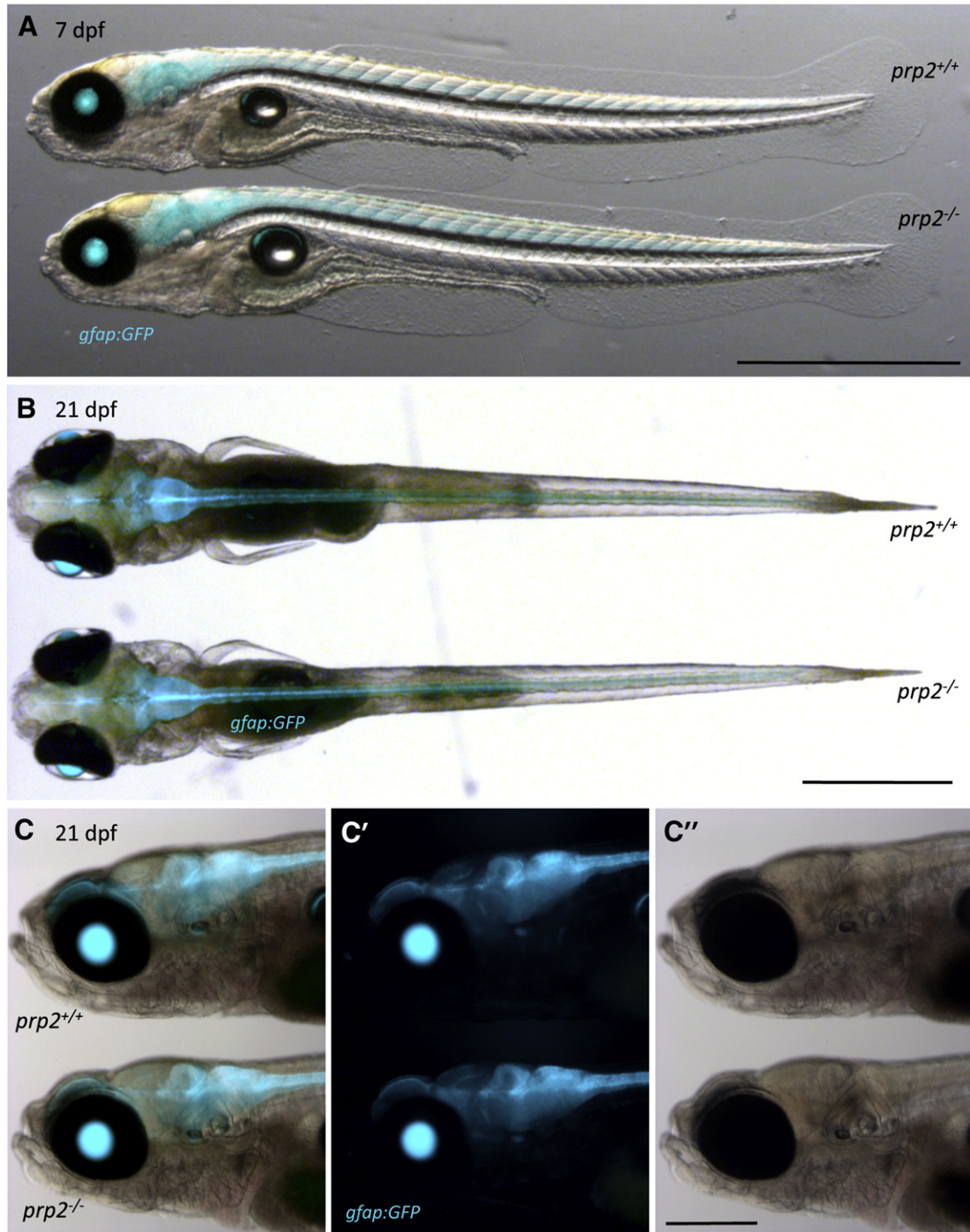


Fig. 4. *Prp2*^{-/-} zebrafish have grossly normal CNS and organ morphology. *prp2*^{-/-} fish were crossed to fish with GFP expressed in the CNS, driven by glial acidic fibrillary protein (GFAP) promoter, on the Casper mutant background that enhances transparency. A. Lateral view of 7 days post-fertilization (dpf) larvae, anterior to the left. GFP expression is not different in intensity or distribution based on genotype. Wild type is on top and *prp2*^{-/-} mutant is on the bottom, and anterior is to the left, throughout the Figure. B. Dorsal view of 21 dpf fish, with GFP revealing normal brain subdivisions and spinal cord in *prp2*^{-/-} fish. C. Lateral view of 21 dpf fish at higher magnification demonstrating GFP distribution in comparison to brightfield, with no detectable differences between genotypes. Alternate views of these fish are presented in Fig. S7. Scale bar = 1 mm in A, B and 0.5 mm in C.

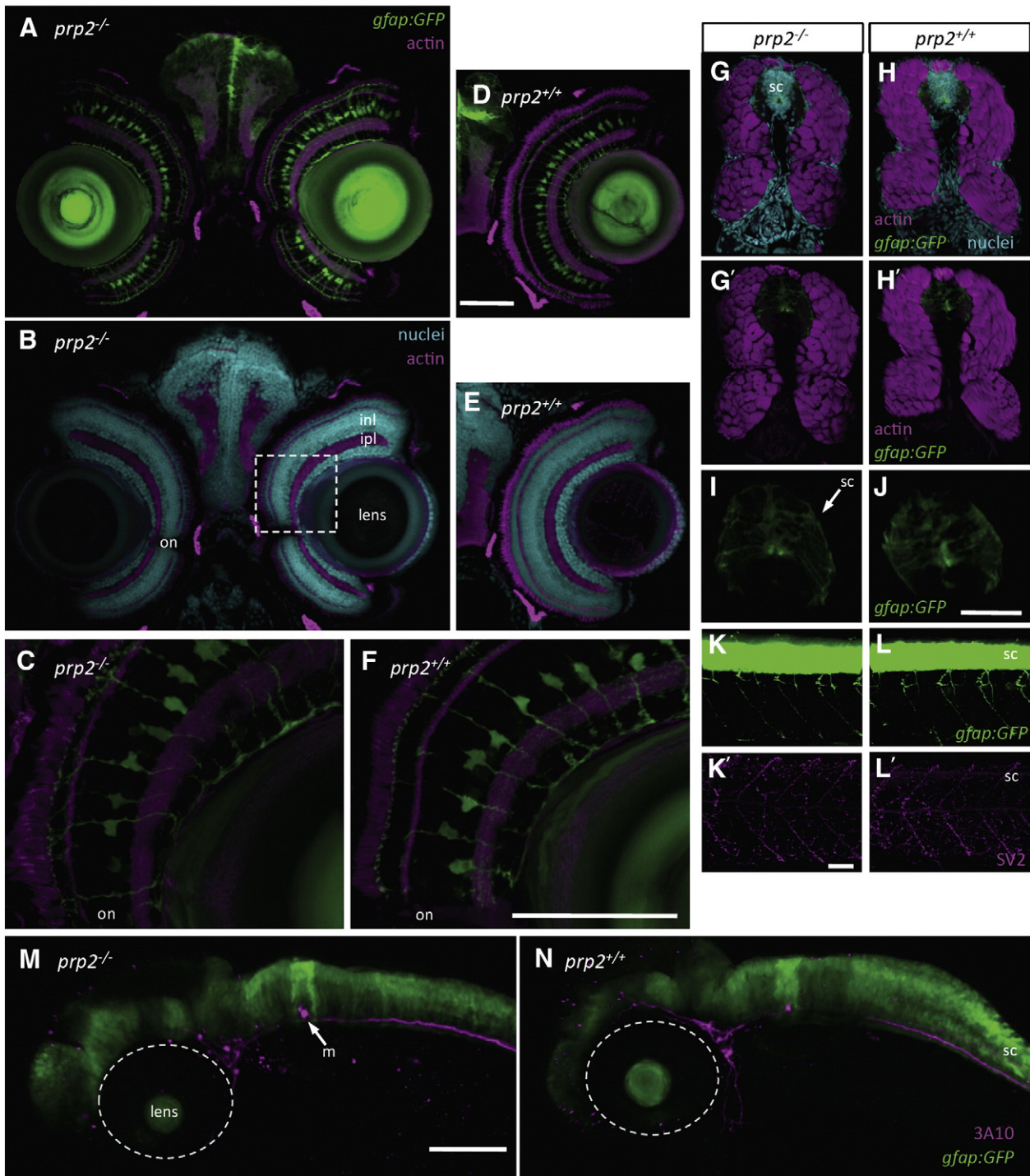


Fig. 5. Histological analysis suggests *prp2*^{-/-} zebrafish have normal CNS organization, polarity and axon guidance. Structures and markers known to be sensitive to degeneration or abnormal development were not observed to be disrupted in *prp2*^{-/-} fish. A–F, Transverse sections through the CNS and eye of mutants (A–C) display normal CNS nuclear and plexiform/synaptic layers, compared to wild type (D–F). Actin staining of synapses shows grossly normal plexiform layers (e.g. inner plexiform layer, ipl; inner nuclear layer, inl). Müller glia filled with GFP are normal in their radial projections and overall morphology. Panels C and F are immediately dorsal of the optic nerve (on), similar to the position boxed by dashed lines in panel B. Dorsal is up in all panels of this figure. G–H, Transverse sections through the trunk musculature and spinal cord (sc). Actin staining emphasizes muscle fascicles with normal organization and nuclei. Radial distribution of glia is normal, as revealed by *gfap:GFP* transgene, with a magnified view in I and J. K, L, Synaptic vesicle (SV2) labeling shows normal motor neuron branching and morphology. Lateral view of trunk, anterior to the left. M, N, A subset of neurons in the head region, labeled with 3A10, have normal axon distribution branching around the eye (outlined with dashed line) from the posterior. The cell bodies of Mauthner neurons (m) are normal, including being embedded in rhombomere four of the hindbrain with intense GFP. Mauthner cell axons project posteriorly in the ventral aspect of the spinal cord. A–J are 7, and K–N are 3 days post-fertilization larvae. Scale bars: A–F, K and L are 50 μ m; G–J are 30 μ m; M, N are 100 μ m.

and that neither was different in its distribution between genotypes (Figs. 5K, L). Labeling with SV2 or 3A10 antibodies in the head region demarcates subpopulations of neurons, and again these were not different between genotypes (Figs. 5M, N). We examined the retina as a

tissue that is readily able to reveal CNS phenotypes in zebrafish larvae due to its rapid development and organized structure. Sections of 7 dpf larval zebrafish eyes appeared normal in *prp2*^{-/-} fish, including normal synaptic and nuclear layers, and unperturbed morphology of

GFP-positive Müller glia that serve various roles including being latent retinal stem cells (Fleisch et al., 2011; Fraser et al., 2013) (Figs. 5A–F).

Disruption of *prp2* produces susceptibility to drug-induced seizures

To characterize the role of *prp2* with respect to neuron function, we assayed if *prp2* loss-of-function leads to increased seizure susceptibility, as has been observed in *Prnp*^{-/-} mice (Carulla et al., 2011; Rangel et al., 2007, 2009; Walz et al., 1999). Zebrafish have often been used in assays of seizure induction and sensitization, enabling testing of pharmacological and/or genetic interventions. We deployed an assay that has been established as a sensitive proxy of seizures (Baraban et al., 2005; Teng et al., 2010), hyperactivity measured as increased total movement of zebrafish larvae following addition of the convulsant PTZ. Examples of the method and tracking of fish movement are shown (Figs. 6A, B and Supplemental Movie 1).

Our primary analysis focused on assessing fish movement during PTZ application, which was normalized to the levels of fish movement prior to PTZ application. The latter can account for inter-individual variability in baseline activity, which can be substantial in larval zebrafish (Shamchuk and Tierney, 2012). Movement representing Stage I and Stage II seizures was increased by approximately 50% in 5 dpf homozygous mutants compared to wild type fish ($p < 0.001$, Fig. 6), indicating that *prp2* plays a role in modulating neuron excitability and seizures. *Prp2*^{ua5001/+} fish were noted to have responses to PTZ that were approximately mid-way between the wild type and *prp2*^{ua5001/ua5001} fish, though this difference was not statistically significant from either genotype (Fig. 6C). Similarly, the average velocity after/before the addition of 2.5 mM PTZ was greater for 3 dpf *prp2*^{ua5001/ua5001} mutants compared to wild type controls (Fig. 6D, $p < 0.05$). In sum, *prp2*^{ua5001/ua5001} fish are induced to hyperactivity by PTZ to a greater extent compared to wild type controls.

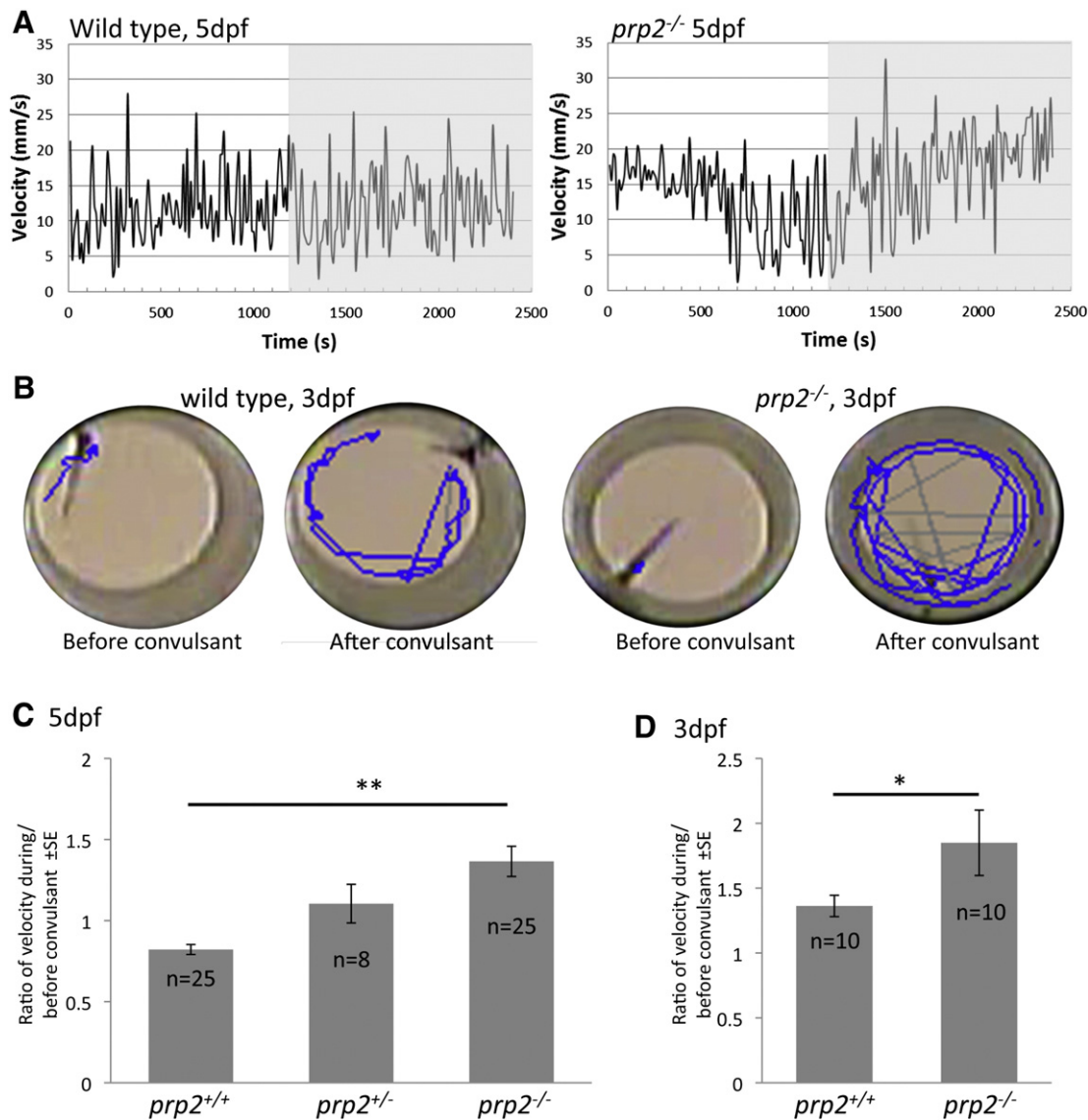


Fig. 6. *Prp2* disruption in zebrafish leads to seizure susceptibility. The convulsant pentylenetetrazol (PTZ, 2.5 mM) increases activity to a greater extent in *prp2*^{-/-} larval fish compared to wild type sibling fish. A. The method involved collecting data traces, examples of which are shown from individual 5 days post-fertilization (dpf) larvae, tracking movement of fish over 20 min, with bath application of PTZ beginning at 1200 s (shaded area). B. Blue lines are example motion paths of 3 dpf *prp2*^{-/-} and *prp2*^{+/+} fish, 5 s in duration, before and during PTZ exposure. Behavior of larvae was monitored in 96-well plates (individual wells shown here, e.g. in 3rd well fish is oriented towards southwest and moved little). Fish of both genotypes exhibited stage I to stage II seizures upon PTZ exposure (defined previously (Baraban et al., 2005, 2007) as a general increase in activity and 'whirlpool' swimming patterns, respectively, also presented in the Supplemental Movie 1). C. Quantifying movement as a proxy of seizures shows that *prp2*^{-/-} fish respond to the PTZ with greater magnitude compared to *prp2*^{+/+} fish. Data are presented as a ratio of velocity during/before PTZ treatment. ** $p < 0.001$ determined with Kruskal–Wallis one-way ANOVA. Raw data presented in Fig. S8. D. Ratio of the average velocity of 3 dpf *prp2*^{-/-} and *prp2*^{+/+} fish during/before treatment with 2.5 mM PTZ. * $p = 0.016$ with the Mann Whitney U-test.

Further analysis was warranted, however, because changes to this after-PTZ/before-PTZ ratio could represent both increased movement of mutants following PTZ or decreased movement of mutants prior to PTZ exposure. Indeed both effects were observed in 5dpf fish, depending on whether maternal mRNA was present during development. Larvae lacking maternal contribution (denoted as 'maternal zygotic' mutants, resulting from breeding *prp2^{ua5001/ua5001}* fish) had substantially lower baseline movement levels compared to wild type fish (Figs. S8A, B), along with the aforementioned increased activity following PTZ (Fig. S8C, $p < 0.001$, $n = 19$). This distinctly contrasted larvae with maternal deposition of *prp2* mRNA (zygotic mutants, resulting from breeding *prp2^{ua5001/+}* fish), where the significant increase in movement with PTZ was observed (Fig. S8C, ratio 1.4, $p < 0.001$, $n = 6$) despite mean velocity prior to PTZ movement being comparable to wild type and heterozygous fish (Fig. S8B). Therefore decreased baseline movement cannot by itself account for the increased ratio of PTZ-induced activity. Maternal zygotic mutants at 3dpf also had reduced baseline movement (Figs. S8D and E). Decreased baseline movement is unto itself a phenotype of interest in the maternal zygotic *prp2^{-/-}* zebrafish.

Overall, *prp2^{-/-}* zebrafish have greater susceptibility to the convulsant compared to wild type fish. No difference was noted regarding induction of increased movement by PTZ when comparing maternal zygotic and zygotic mutant fish, suggesting that maternal contributions of *prp2* mRNA were inert towards the PTZ-induced seizure-like phenotype. Similar results from *Prnp^{-/-}* mice suggest that PrP^C has a deeply conserved role in modulating neuron excitability.

NMDA receptor kinetics are altered in *prp2^{-/-}* larvae

Having observed an increase in seizure susceptibility, it was of interest to consider if neurophysiological changes at the level of the synapse might correlate with the altered behavior. PrP^C is known to regulate the activity of various channels, including nicotinic acetylcholine receptors, AMPA receptors and voltage gated potassium channels (Alier et al., 2011; Beraldo et al., 2010; Khosravani et al., 2008b). NMDA channels were of particular interest due to their known role in PTZ-mediated behavioral effects in mice (though other channels are also involved), and the potential linkage of PrP to deregulation of NMDA receptors leading to excitotoxicity (Khosravani et al., 2008a; Stys et al., 2012; You et al., 2012).

Spontaneous synaptic NMDA receptor currents were analyzed for a number of properties. Patch-clamp recordings were used to document miniature excitatory post-synaptic currents (mEPSCs) from the Mauthner neuron in the intact hindbrain of wild type and maternal zygotic *prp2^{-/-}* zebrafish. The Mauthner neuron is reliably recognizable by light microscopy, and its activity controls swimming behaviors in the larval fish. Glutamate excitatory currents, representing AMPA and NMDA receptors, were isolated using pharmacology and acquired at holding potentials of -60 mV and $+40$ mV, but NMDA currents were only apparent at positive potentials that relieve Mg^{2+} block of the channel. The accurate identification of NMDA synaptic currents was confirmed, since they were not observable upon addition of the NMDA receptor antagonist APV in either wild type or *prp2^{-/-}* fish (Fig. 7A). Washout of APV resulted in the re-appearance of NMDA mEPSCs, and AMPA currents remained observable throughout. Characterizing NMDA currents in each genotype demonstrated no significant difference in amplitude (Fig. 7D, $p = 0.75$, $n = 4$ and $n = 7$ embryos), but NMDA currents occurred with lower frequency in *prp2^{-/-}* embryos compared to wild type (Fig. 7C, $p = 0.026$, $n = 6$ and $n = 10$ embryos, respectively). It is noteworthy that these currents represent spontaneous events, rather than evoked events, and thus changes in frequency may or may not be due to altered Mauthner neuron excitability. Kinetics of NMDA receptors were considered next, as these are altered in brain slices from *Prnp^{-/-}* mice (Khosravani et al., 2008a; You et al., 2012). Rise time of NMDA mEPSCs was not different between genotypes

($p = 0.62$) but the decay time was. The increase in decay time is evident in averaged example traces (Fig. 7B). The kinetics of mEPSC decay time were best fit with a tandem of exponential curves consisting of a fast and a slow component, τ_1 and τ_2 respectively. In particular, τ_1 was not different ($p = 0.14$) but τ_2 was doubled in *prp2^{-/-}* fish (Fig. 7C, $p < 0.001$, $n = 7$ wild type, $n = 4$ *prp2^{-/-}* larvae, with 10 to 68 traces being averaged per recording). Immunohistochemistry and confocal microscopy failed to reveal a difference in Mauthner cell morphology (Figs. 7H, I and 5M, N).

The observations regarding *prp2* disruption affecting NMDA receptor kinetics were independently confirmed in wild type zebrafish injected with *prp2* morpholino. This included co-injection of *p53* morpholino to suppress off-target effects (as discussed above, see Figs. S6E, S6F regarding *p53* MO inclusion). The comparator larvae were injected with an equal dose of a standard control MO and *p53* MO. The recordings used in the morphant analysis included mixed AMPA and NMDA receptor currents. Thus the very fast decay component in the morphant experiments represents AMPA receptor activity, whereas the slow decay component is dominated by the NMDA receptors comparable to the τ_2 component that was altered in the *prp2^{-/-}* larvae above. The slow NMDA component was more evident in the *prp2* morphants compared with the controls (Fig. S9 panel A' vs. A). The slow component was doubled in *prp2* MO fish ($p < 0.05$, $n = 3$ fish per genotype) with no observed change in amplitude (Fig. S9).

In sum, results using two gene disruption technologies and two sets of recording parameters each revealed that the NMDA channels in *prp2^{-/-}* fish have altered kinetics: once opened, NMDA receptors remain open longer. This predicts a protective role for Prp2, preventing excitotoxicity during neuronal insult, and accords well with increased neuron excitability that is presumed to be causal of the increased seizure susceptibility reported above (Fig. 6).

Discussion

Knockout of the *Prnp* gene in mice has been fundamental to understanding of prion disease etiology, allowing confirmation that the gene product is crucial to prion disease progression (Prusiner, 1991). Furthermore, this knockout background has enabled the engineering of transgenic mice that can be infected with prion disease isolates from various species, propelling the study of various impactful prionopathies. *Prnp^{-/-}* mice develop normally, and display few adult phenotypes (Bueler et al., 1992). This has hampered assignment of a function to PrP, a conserved protein that is highly abundant in healthy brains (Aguzzi et al., 2008). Thus we were deeply intrigued by findings that a tractable animal model, the zebrafish, presents with a robust neurodevelopmental phenotype during knockdown of either of two *Prnp* homologs (Kaiser et al., 2012; Malaga-Trillo et al., 2009; Nourizadeh-Lillabadi et al., 2010). This previous work utilized morpholino technology that permits only transient (multi-day) and partial knockdown of prion protein translation. We sought to confirm these results using an independent method of disrupting the prion gene.

We deployed an emerging technology, zinc finger nucleases, because such approaches have promise to enable targeted mutation of most genes in zebrafish. Use of ZFNs in zebrafish was recently pioneered by three groups (Amacher, Joung, Wolfe and Lawson, see (Doyon et al., 2008; Ekker, 2008; Foley et al., 2009; McCammon et al., 2011; Meng et al., 2008; Sander et al., 2011; Zhu et al., 2011)) who have been generous in sharing their reagents and experience. The current results represent a rare success deploying ZFN technology in zebrafish beyond the aforementioned groups (see also Ben et al., 2011), thus validating the tractability of the targeted mutagenesis approach for the broader zebrafish community.

We generated zebrafish with a frame-shift mutation early in the prion protein gene 2 (*prp2*) and find that the fish lacks overt phenotypes. This is consistent with the lack of overt phenotypes when PrP

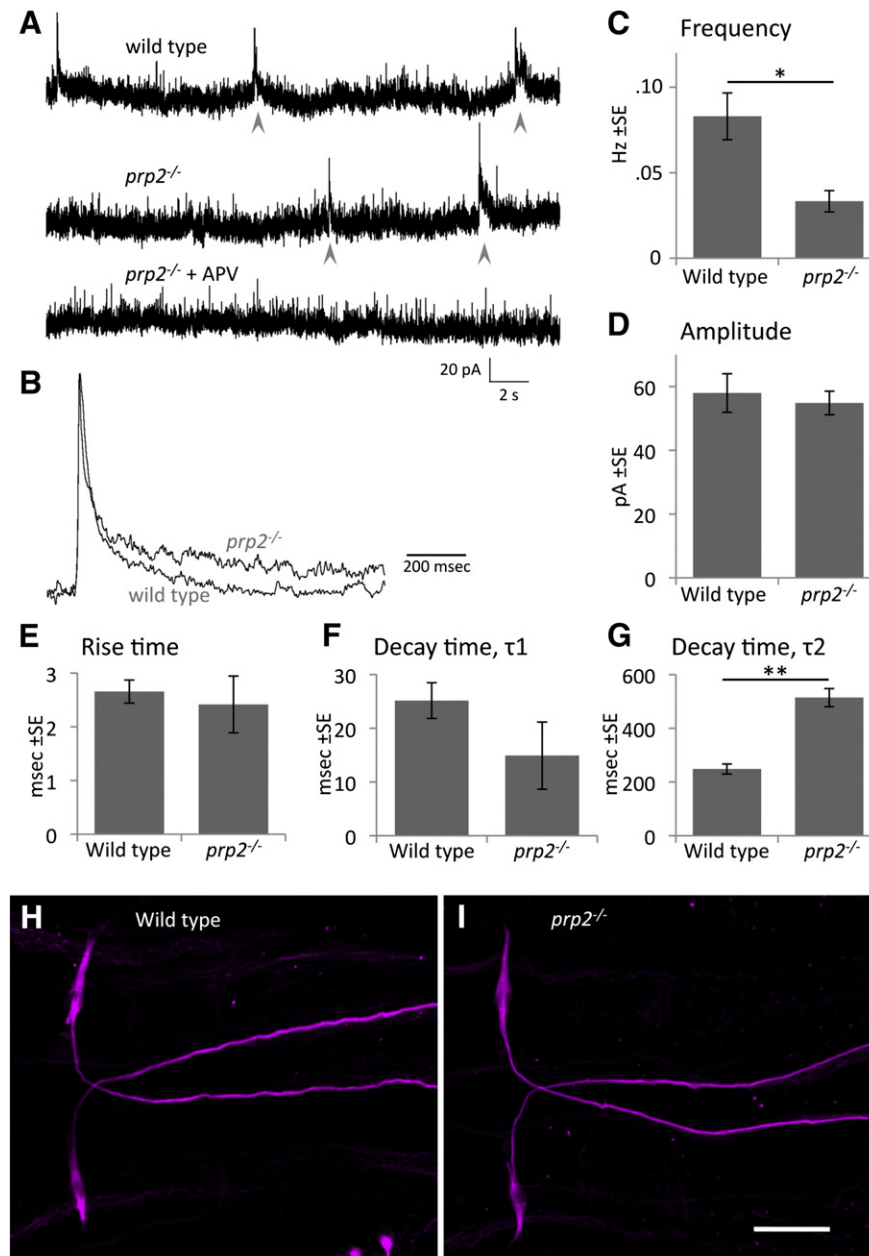


Fig. 7. *Prp2* regulates N-Methyl-D-aspartate (NMDA) Receptor currents in vivo. **A.** Glutamate miniature excitatory post-synaptic currents (mEPSCs) recorded from individual Mauthner cells in the intact zebrafish hindbrain. Example traces are from wild type and *prp2*^{-/-} larvae (top and middle, respectively). The bottom trace confirms identification of NMDA mEPSCs (arrowheads) since they are absent upon addition of the NMDA receptor antagonist, APV. Smaller events in the traces are AMPA mEPSCs. **B.** Averaged NMDA mEPSCs obtained from wild type and *prp2*^{-/-} larvae. It is apparent that the NMDA receptors in *prp2*^{-/-} fish (top) take longer to return to baseline. Traces are normalized to an equivalent amplitude to permit comparison of receptor kinetics. **C.** The frequency of NMDA responses is significantly lower in *prp2*^{-/-} larvae compared to wild type ($p < 0.05$, $n = 6$ and $n = 10$, respectively). **D, E.** NMDA receptor potentials in wild type and *prp2*^{-/-} larvae do not measurably differ in amplitude or rise time. **F, G.** Decay time is fit with two exponential components, τ_1 and τ_2 , to best represent the kinetics of channel closure. The second component, τ_2 (panel G), is significantly greater in *prp2*^{-/-} larvae compared to wild type (** $p < 0.001$, $n = 4$ and $n = 7$ fish respectively for panels D–G, with multiple events averaged per fish). Thus NMDA channels stay open longer (e.g. see panel B) when *prp2* is disrupted in zebrafish. This was confirmed in *prp2* morphants (Fig. S9). **H, I.** Mauthner cell morphology is not detectably different in wild type vs. *prp2*^{-/-} larvae. Dorsal view of zebrafish hindbrain, anterior to the left, with two Mauthner cell bodies and axons projecting contralaterally across the midline in each fish. Scale bar = 50 μm .

is disrupted in mice (Bueler et al., 1992) and other mammals (Richt et al., 2007; Yu et al., 2009). Our data suggest the discrepancy between the zebrafish *prp2* mutant and morphant can be attributed to a lack of specificity in the morpholino reagents deployed. This is likely to emerge as a common theme in zebrafish biology, as the tractable morpholino technology is slowly supplanted by laborious targeted mutation and gene tilling mutagenesis projects.

The normal development of zebrafish lacking *prp2* contrasts the gastrulation and CNS cell death effects observed following knockdown of *prp1* in zebrafish using morpholinos (Kaiser et al., 2012; Malaga-Trillo et al., 2009). Future work is needed to decipher if this difference is

attributable to the technologies used, the gene products involved (e.g. differences in amino acid sequences) and/or differences in their expression. The latter explanation is probable, in that *prp1* is expressed in most cells and very early in development, whereas *prp2* expression becomes more robust later in development and is primarily restricted to the CNS.

Characterizing the *prp2*^{-/-} fish generated herein using behavioral and electrophysiological paradigms confirmed that PrP plays a conserved, and thus important role in regulating neuron excitability. Recent work has suggested that PrP acts to modulate channel excitability in neurons, consistent with its roles in synaptogenesis and neuroprotection (modulating excitotoxicity). The current evidence

extends these findings to an in vivo paradigm and argues that regulation of ion channels is an ancient function of this protein. This is consistent with this abundant protein having a homeostatic role that comes to the forefront during insults to the CNS.

Alterations to NMDA receptor decay kinetics have been found in brain slices comparing wild type and *Prnp*^{-/-} mice (Khosravani et al., 2008a; You et al., 2012). The data herein closely parallel this work, including a marked slowing of NMDA receptor deactivation. Other studies indicate *Prnp*^{-/-} mice have altered abundance of transcripts encoding NMDA receptor (Maglio et al., 2004), and NMDA receptors participate in their increased susceptibility to kainate-induced cell death (Rangel et al., 2007). Here, a role for the prion protein in modulating NMDA receptor kinetics has been confirmed in situ. This deep conservation suggests it as an ancient role for the prion protein in modulating NMDA receptors and neuron excitability.

Decreased baseline movement was observed prior to addition of convulsant in the 5 dpf maternal zygotic *prp2*^{-/-} zebrafish (lacking maternal contribution of *prp2* mRNA into the egg), suggesting that *prp2* plays at least two roles with respect to zebrafish movement. First, lack of *prp2* affects early development in some fashion that later manifests as decreased basal movement/lethargy in the fish. This is in accord with the decreased frequency of spontaneous NMDA events in maternal zygotic *prp2*^{-/-} fish. Second, lack of *prp2* has an acute effect on zebrafish behavioral susceptibility to the convulsant PTZ, regardless of maternal contributions of *prp2* mRNA. This acute effect is in good accordance with altered kinetics of NMDA receptor closure in *prp2*^{-/-} fish. Future work is required to test whether the observed alterations to NMDA receptor currents cause the observed changes in activity and seizure susceptibility.

The regulation of NMDA receptors by the prion protein PrP^C has recently been demonstrated to be mechanistically linked, at least in part, to PrP^C modulating copper availability (Khosravani et al., 2008a; You et al., 2012). PrP^C is a potent regulator of copper homeostasis (Millhauser, 2007), and copper abundance is a well-established effector of NMDA receptor kinetics (reviewed in Stys et al., 2012). Recent work integrates a role for amyloid β oligomers ($A\beta$ oligomers accumulate in Alzheimer disease) in this regulation, such that $A\beta$ chelates copper availability away from the PrP^C-NMDA receptor interaction (You et al., 2012). Considering the prion protein homologs in zebrafish, this conclusion is intriguing on at least two levels. First, some of us have recently reported that zebrafish *prp1* genetically interacts with the $A\beta$ precursor protein (APP) holoprotein, and extended this by demonstrating biochemical interactions of human PrP^C-APP in vitro (Kaiser et al., 2012). These observations broaden the landscape of PrP^C-APP interactions that might prove to be relevant to disease etiology. Second, the regulation of copper abundance at NMDA receptors in mammals is presumed to revolve around PrP's octarepeat region, yet this region is substantively different in zebrafish. The octarepeats (PHGGGWGQ) of mammalian PrP^C coordinate copper binding at histidine residues in each repeat. The equivalent domain of zebrafish Prp2 protein is homologous, including being unambiguously repetitive (containing multiple PxxxxY motifs, Fig. S1), yet none of the repeats in zebrafish Prp2 possess known signatures of copper binding. Thus both mammalian and zebrafish PrP proteins modulate NMDA receptor kinetics in a very similar fashion, but only the former is likely to modulate copper via the repetitive region. This is worthy of further pursuit, as understanding the role of PrP^C and copper has the potential to inform both prion and Alzheimer disease therapeutics, wherein NMDA receptor antagonists are in clinical trial (Olivares et al., 2012).

In this light, it is intriguing that prion proteins are now understood to have evolved from the transmembrane zip proteins with ancient functions in copper and zinc transport (Ehsani et al., 2011, 2012; Schmitt-Ulms et al., 2009). Mammalian PrP^C and Zip proteins interact in a hypothesized role of modulating divalent cations (Ehsani et al., 2011, 2012; Schmitt-Ulms et al., 2009). It is striking that PrP in a basal vertebrate may share fundamental PrP functions at the synapse, while

apparently lacking core metal homeostatic properties. It will be of interest to understand the role of zebrafish Prp2 with respect to copper homeostasis as this may provide insights into both NMDA receptor-based therapeutics and the evolution of the zip/prion protein family and their myriad mechanisms impinging upon synaptic metal homeostasis.

Supplementary data to this article can be found online at <http://dx.doi.org/10.1016/j.nbd.2013.03.007>.

Acknowledgments

We thank Scot Wolfe for reagents and very valuable feedback on the ZFN technology. We appreciate the advice of David Westaway regarding an earlier version of this manuscript. We are grateful to Aleah McCorry for assistance with fish husbandry and Angela Shamchuk for assistance with behavior tracking. This work was supported by Alberta Prion Research Institute, Alberta Innovates – Bio Solutions [AIF APRI 200800739 to WTA]; Alzheimer Society of Canada [to WTA]; PrioNet Canada, a Networks of Centres of Excellence Canada [NCEPNC HIF Allison to WTA]; Canadian Institutes of Health Research [CHRPJ 365482-2009 to AJW and WTA]; and Natural Sciences and Engineering Research Council of Canada [CHRPJ 365482-2009 to AJW and WTA, RGPIN 371928-09 to WTA; RGPIN 298371-2010 to AJW; RGPIN 238569-2011 to DWA]. Salary support was provided by Alzheimer Society of Canada [PLAL]; Alberta Heritage Foundation for Medical Research [LMP]; and Swiss National Science Foundation [VCF].

References

- Aguzzi, A., et al., 2008. The prion's elusive reason for being. *Annu. Rev. Neurosci.* 31, 439–477.
- Alier, K., et al., 2011. Abeta inhibition of ionic conductance in mouse basal forebrain neurons is dependent upon the cellular prion protein PrP^C. *J. Neurosci.* 31, 16292–16297.
- Allison, W.T., et al., 2010. Ontogeny of cone photoreceptor mosaics in zebrafish. *J. Comp. Neurol.* 518, 4182–4195.
- Baraban, S.C., et al., 2005. Pentylentetrazole induced changes in zebrafish behavior, neural activity and c-fos expression. *Neuroscience* 131, 759–768.
- Baraban, S.C., et al., 2007. A large-scale mutagenesis screen to identify seizure-resistant zebrafish. *Epilepsia* 48, 1151–1157.
- Bedell, V.M., et al., 2011. Lessons from morpholino-based screening in zebrafish. *Brief. Funct. Genomics* 10, 181–188.
- Ben, J., et al., 2011. Targeted mutation of the talpid3 gene in zebrafish reveals its conserved requirement for ciliogenesis and hedgehog signalling across the vertebrates. *Development* 138, 4969–4978.
- Beraldo, F.H., et al., 2010. Role of alpha7 nicotinic acetylcholine receptor in calcium signaling induced by prion protein interaction with stress-inducible protein 1. *J. Biol. Chem.* 285, 36542–36550.
- Bernardos, R.L., Raymond, P.A., 2006. GFAP transgenic zebrafish. *Gene Expression Patterns* 6, 1007–1013.
- Bhinder, G., Tierney, K.B., 2012. Olfactory-evoked activity assay for larval zebrafish. *Zebrafish Protoc. Neurobehav. Res.* 71–84.
- Bueler, H., et al., 1992. Normal development and behaviour of mice lacking the neuronal cell-surface PrP protein. *Nature* 356, 577–582.
- Bustin, S.A., et al., 2009. The MIQE guidelines: minimum information for publication of quantitative real-time PCR experiments. *Clin. Chem.* 55, 611–622.
- Carulla, P., et al., 2011. Neuroprotective role of PrP against kainate-induced epileptic seizures and cell death depends on the modulation of JNK3 activation by GluR6/7-PSD-95 binding. *Mol. Biol. Cell.* 22, 3041–3054.
- Casadei, R., et al., 2011. Identification of housekeeping genes suitable for gene expression analysis in the zebrafish. *Gene Expr. Patterns* 11, 271–276.
- Cotto, E., et al., 2005. Molecular characterization, phylogenetic relationships, and developmental expression patterns of prion genes in zebrafish (*Danio rerio*). *FEBS J.* 272, 500–513.
- Culbertson, M.R., 1999. RNA surveillance. Unforeseen consequences for gene expression, inherited genetic disorders and cancer. *Trends Genet.* 15, 74–80.
- Daude, N., et al., 2012. Knockout of the prion protein (PrP)-like Sprn gene does not produce embryonic lethality in combination with PrP^C-deficiency. *Proc. Natl. Acad. Sci. U. S. A.*
- Doyon, Y., et al., 2008. Heritable targeted gene disruption in zebrafish using designed zinc-finger nucleases. *Nat. Biotechnol.* 26, 702–708.
- Ehsani, S., et al., 2011. Family reunion—the ZIP/prion gene family. *Prog. Neurobiol.* 93, 405–420.
- Ehsani, S., et al., 2012. LIV-1 ZIP ectodomain shedding in prion-infected mice resembles cellular response to transition metal starvation. *J. Mol. Biol.*
- Eisen, J.S., Smith, J.C., 2008. Controlling morpholino experiments: don't stop making antisense. *Development* 135, 1735–1743.
- Ekker, S.C., 2008. Zinc finger-based knockout punches for zebrafish genes. *Zebrafish* 5, 121–123.

- Fleisch, V.C., et al., 2011. Investigating regeneration and functional integration of CNS neurons: lessons from zebrafish genetics and other fish species. *Biochim. Biophys. Acta* 1812, 364–380.
- Foley, J.E., et al., 2009. Rapid mutation of endogenous zebrafish genes using zinc finger nucleases made by Oligomerized Pool ENgineering (OPEN). *PLoS One* 4, e4348.
- Fraser, B., et al., 2013. Regeneration of cone photoreceptors when cell ablation is primarily restricted to a particular cone subtype. *PLoS One* 8, e55410.
- Hatta, K., et al., 1991. Diversity of expression of engrailed-like antigens in zebrafish. *Development* 112, 821–832.
- Jost, C.A., et al., 1997. p73 is a simian [correction of human] p53-related protein that can induce apoptosis. *Nature* 389, 191–194.
- Kaiser, D.M., et al., 2012. Amyloid β precursor protein and prion protein have a conserved interaction affecting cell adhesion and CNS development. *PLoS One* 7, e51305.
- Khalife, M., et al., 2011. Transcriptomic analysis brings new insight into the biological role of the prion protein during mouse embryogenesis. *PLoS One* 6, e23253.
- Khosravani, H., et al., 2008a. Prion protein attenuates excitotoxicity by inhibiting NMDA receptors. *J. Cell Biol.* 181, 551–565.
- Khosravani, H., et al., 2008b. Cellular prion protein null mice display normal AMPA receptor mediated long term depression. *Prion* 2, 48–50.
- Langheinrich, U., et al., 2002. Zebrafish as a model organism for the identification and characterization of drugs and genes affecting p53 signaling. *Curr. Biol.* 12, 2023–2028.
- Lauren, J., et al., 2009. Cellular prion protein mediates impairment of synaptic plasticity by amyloid-beta oligomers. *Nature* 457, 1128–1132.
- Lemmens, R., et al., 2007. Overexpression of mutant superoxide dismutase 1 causes a motor axonopathy in the zebrafish. *Hum. Mol. Genet.* 16, 2359–2365.
- Maglio, L.E., et al., 2004. Hippocampal synaptic plasticity in mice devoid of cellular prion protein. *Brain Res. Mol. Brain Res.* 131, 58–64.
- Malaga-Trillo, E., et al., 2009. Regulation of embryonic cell adhesion by the prion protein. *Plos Biol.* 7, 576–590.
- Manson, J.C., et al., 1994. 129/Ola mice carrying a null mutation in PrP that abolishes mRNA production are developmentally normal. *Mol. Neurobiol.* 8, 121–127.
- Maquat, L.E., 2004. Nonsense-mediated mRNA decay: splicing, translation and mRNP dynamics. *Nat. Rev. Mol. Cell Biol.* 5, 89–99.
- McCammon, J.M., et al., 2011. Inducing high rates of targeted mutagenesis in zebrafish using zinc finger nucleases (ZFNs). *Methods Mol. Biol.* 770, 505–527.
- Meng, X.D., et al., 2008. Targeted gene inactivation in zebrafish using engineered zinc finger nucleases. *Nat. Biotechnol.* 26, 695–701.
- Middeldorp, J., Hol, E.M., 2011. GFAP in health and disease. *Prog. Neurobiol.* 93, 421–443.
- Miesbauer, M., et al., 2006. Prion protein-related proteins from zebrafish are complex glycosylated and contain a glycosylphosphatidylinositol anchor. *Biochem. Biophys. Res. Commun.* 341, 218–224.
- Millhauser, G.L., 2007. Copper and the prion protein: methods, structures, function, and disease. *Annu. Rev. Phys. Chem.* 58, 299–320.
- Nourizadeh-Lillabadi, R., et al., 2010. Early embryonic gene expression profiling of zebrafish prion protein (Prp2) morphants. *PLoS One* 5, e13573.
- Olivares, D., et al., 2012. N-methyl D-aspartate (NMDA) receptor antagonists and memantine treatment for Alzheimer's disease, vascular dementia and Parkinson's disease. *Curr. Alzheimer Res.* 9, 746–758.
- Patten, S.A., Ali, D.W., 2009. PKCgamma-induced trafficking of AMPA receptors in embryonic zebrafish depends on NSF and PICK1. *Proc. Natl. Acad. Sci. U. S. A.* 106, 6796–6801.
- Patten, S.A., et al., 2010. Protein kinase Cgamma is a signaling molecule required for the developmental speeding of alpha-amino-3-hydroxyl-5-methyl-4-isoxazole-propionate receptor kinetics. *Eur. J. Neurosci.* 31, 1561–1573.
- Prusiner, S.B., 1991. Molecular biology of prion diseases. *Science* 252, 1515–1522.
- Rangel, A., et al., 2007. Enhanced susceptibility of Prnp-deficient mice to kainate-induced seizures, neuronal apoptosis, and death: role of AMPA/kainate receptors. *J. Neurosci. Res.* 85, 2741–2755.
- Rangel, A., et al., 2009. Regulation of GABA(A) and glutamate receptor expression, synaptic facilitation and long-term potentiation in the hippocampus of prion mutant mice. *PLoS One* 4, e7592.
- Richt, J.A., et al., 2007. Production of cattle lacking prion protein. *Nat. Biotechnol.* 25, 132–138.
- Robu, M.E., et al., 2007. p53 activation by knockdown technologies. *PLoS Genet.* 3, e78.
- Sander, J.D., et al., 2011. Selection-free zinc-finger-nuclease engineering by context-dependent assembly (CoDA). *Nat. Methods* 8, 67–69.
- Schmitt-Ulms, G., et al., 2009. Evolutionary descent of prion genes from the ZIP family of metal ion transporters. *PLoS One* 4, e7208.
- Shamchuk, A.L., Tierney, K.B., 2012. Phenotyping stimulus evoked responses in larval zebrafish behaviour. *Behaviour* 149, 1177–1203.
- Steele, A.D., et al., 2007. The prion protein knockout mouse: a phenotype under challenge. *Prion* 1, 83–93.
- Stys, P.K., et al., 2012. Copper-dependent regulation of NMDA receptors by cellular prion protein: implications for neurodegenerative disorders. *J. Physiol.* 590, 1357–1368.
- Tang, R., et al., 2007. Validation of zebrafish (*Danio rerio*) reference genes for quantitative real-time RT-PCR normalization. *Acta Biochim. Biophys. Sin. (Shanghai)* 39, 384–390.
- Teng, Y., et al., 2010. Knockdown of zebrafish Lgi1a results in abnormal development, brain defects and a seizure-like behavioral phenotype. *Hum. Mol. Genet.* 19, 4409–4420.
- Walz, R., et al., 1999. Increased sensitivity to seizures in mice lacking cellular prion protein. *Epilepsia* 40, 1679–1682.
- Westerfield, M., 2000. *The Zebrafish Book. A Guide for the Laboratory Use of Zebrafish (Danio rerio)*. University of Oregon Press, Eugene, OR.
- White, R.M., et al., 2008. Transparent adult zebrafish as a tool for in vivo transplantation analysis. *Cell Stem Cell* 2, 183–189.
- Wittkopp, N., et al., 2009. Nonsense-mediated mRNA decay effectors are essential for zebrafish embryonic development and survival. *Mol. Cell. Biol.* 29, 3517–3528.
- Yazulla, S., Studholme, K.M., 2001. Neurochemical anatomy of the zebrafish retina as determined by immunocytochemistry. *J. Neurocytol.* 30, 551–592.
- You, H., et al., 2012. Abeta neurotoxicity depends on interactions between copper ions, prion protein, and N-methyl-D-aspartate receptors. *Proc. Natl. Acad. Sci. U. S. A.* 109, 1737–1742.
- Yu, G., et al., 2009. Generation of goats lacking prion protein. *Mol. Reprod. Dev.* 76, 3.
- Zhu, C., et al., 2011. Evaluation and application of modularly assembled zinc-finger nucleases in zebrafish. *Development* 138, 4555–4564.